

**NRL Report 6806**

**Sea-Clutter Measurements on Four Frequencies**

**John C. Daley, John T. Ransone, Jr., Joseph A. Burkett, and James R. Duncan**

*Wave Propagation Branch  
Electronics Division*

**November 29, 1968**



Approved for Public Release  
Distribution Unlimited

**Naval Research Laboratory  
Washington, D.C.**

**NRL Report 6806**

**Sea-Clutter Measurements on Four Frequencies**

**John C. Daley, John T. Ransone, Jr., Joseph A. Burkett, and James R. Duncan**

*Wave Propagation Branch  
Electronics Division*

**November 29, 1968**



Approved for Public Release  
Distribution Unlimited

**Naval Research Laboratory  
Washington, D.C.**

## DOCUMENT CONTROL DATA - R &amp; D

(Security classification of title, body of abstract and indexing annotation must be entered when the overall report is classified)

1. ORIGINATING ACTIVITY (Corporate author)		2a. REPORT SECURITY CLASSIFICATION	
Naval Research Laboratory Washington, D. C. 20390		Unclassified	
		2b. GROUP	
3. REPORT TITLE			
SEA-CLUTTER MEASUREMENTS ON FOUR FREQUENCIES			
4. DESCRIPTIVE NOTES (Type of report and inclusive dates)			
Interim report; work is continuing on the problem			
5. AUTHOR(S) (First name, middle initial, last name)			
John C. Daley, John T. Ransone, Jr., Joseph A. Burkett, and James R. Duncan			
6. REPORT DATE		7a. TOTAL NO. OF PAGES	7b. NO. OF REFS
November 29, 1968		46	19
8a. CONTRACT OR GRANT NO.		9a. ORIGINATOR'S REPORT NUMBER(S)	
NRL Problem R02-37		NRL Report 6806	
b. PROJECT NO.			
A31-533/652/69R008-01-020			
c.		9b. OTHER REPORT NO(S) (Any other numbers that may be assigned this report)	
d.			
10. DISTRIBUTION STATEMENT			
This document is subject to special export controls and each transmittal to foreign nationals may be made only with prior approval of the Director, Naval Research Laboratory, Washington, D. C. 20390.			
11. SUPPLEMENTARY NOTES		12. SPONSORING MILITARY ACTIVITY	
		Department of the Navy (Naval Air Systems Command), Washington, D. C. 20360	
13. ABSTRACT			
<p>The initial processing and analysis of radar backscatter data, recorded off the coast of San Juan, Puerto Rico, in July 1965, have been completed. This data constituted part of a study conducted in conjunction with the Applied Physics Laboratory (APL) of Johns Hopkins University to determine the scattering mechanism involved in the generation of sea clutter. The NRL WV-2 instrumented aircraft with its four-frequency, pulsed radar system and a surface vessel equipped and staffed by APL to gather sea-surface data in the form of stereophotographs and wave-buoy measurements were used in this experiment.</p> <p>Radar returns were collected nearly simultaneously on four frequencies: 428 MHz, 1228 MHz, 4455 MHz, 8910 MHz, for both linear and cross polarizations. The data were processed to obtain the normalized radar cross section <math>\sigma_0</math> of the sea surface as a function of various parameters. In particular, the behavior of the median value of the cross section <math>\sigma_0</math> was investigated as a function of wind direction, incident angle, polarization, radar wavelength, and gross surface conditions of wind velocity and wave height. Results are given for the upwind direction and the linear polarization (vertical and horizontal). The polarization ratio is shown to decrease with increasing sea roughness and to be a function of radar wavelength. As surface roughness increases, <math>\sigma_0</math> becomes independent of wavelength for vertical polarization but maintains an inverse wavelength dependence for horizontal polarization. The results given provide estimates of <math>\sigma_0</math> as a function of the above parameters over an angular range of 4 to 90 degrees (vertical incidence) and from calm sea conditions to moderately rough conditions characterized by 5- to 7-foot wave heights and 10- to 20-knot winds.</p>			

14. KEY WORDS	LINK A		LINK B		LINK C	
	ROLE	WT	ROLE	WT	ROLE	WT
Sea clutter Sea-clutter scattering Sea-surface measurements Radar Oceanography						

## CONTENTS

Abstract	ii
Problem Status	ii
Authorization	ii
INTRODUCTION	1
INSTRUMENTATION	2
DATA COLLECTION AND PROCESSING	5
DATA PRESENTATION	6
DEPENDENCE OF $\sigma_0$ ON INCIDENT ANGLE	9
DEPENDENCE OF SEA CLUTTER ON SEA STATE	9
DEPENDENCE OF SEA CLUTTER ON POLARIZATION	24
DEPENDENCE OF SEA CLUTTER ON WAVELENGTH	24
SYSTEM LIMITATIONS	25
CONCLUSIONS	39
FUTURE WORK	40
REFERENCES	41

## ABSTRACT

The initial processing and analysis of radar backscatter data, recorded off the coast of San Juan, Puerto Rico, in July 1965, have been completed. This data constituted part of a study conducted in conjunction with the Applied Physics Laboratory (APL) of Johns Hopkins University to determine the scattering mechanism involved in the generation of sea clutter. The NRL WV-2 instrumented aircraft with its four-frequency, pulsed radar system and a surface vessel equipped and staffed by APL to gather sea-surface data in the form of stereophotographs and wave-buoy measurements were used in this experiment.

Radar returns were collected nearly simultaneously on four frequencies: 428 MHz, 1228 MHz, 4455 MHz, 8910 MHz, for both linear and cross polarizations. The data were processed to obtain the normalized radar cross section  $\sigma_0$  of the sea surface as a function of various parameters. In particular, the behavior of the median value of the cross section  $\sigma_0$  was investigated as a function of wind direction, incident angle, polarization, radar wavelength, and gross surface conditions of wind velocity and wave height. Results are given for the upwind direction and the linear polarization (vertical and horizontal). The polarization ratio is shown to decrease with increasing sea roughness and to be a function of radar wavelength. As surface roughness increases,  $\sigma_0$  becomes independent of wavelength for vertical polarization but maintains an inverse wavelength dependence for horizontal polarization. The results given provide estimates of  $\sigma_0$  as a function of the above parameters over an angular range of 4 to 90 degrees (vertical incidence) and from calm sea conditions to moderately rough conditions characterized by 5- to 7-foot wave heights and 10- to 20-knot winds.

## PROBLEM STATUS

This is an interim report on this problem.

## AUTHORIZATION

NRL Problem R02-37  
Project A31-533/652/69R008-01-020

Manuscript submitted September 16, 1968.

## SEA-CLUTTER MEASUREMENTS ON FOUR FREQUENCIES

### INTRODUCTION

A quantitative description of radar sea clutter has long been sought, first, by the radar designer who must predict system performance in terms of detection probabilities of targets in a clutter background and, second, by the oceanographer who would like to estimate surface characteristics from the radar return. In the first case, the designer would reduce the effect of clutter on the target return. In the second case, the clutter itself is wanted as an indicator of the environment. In both cases, a useful measurement is the absolute magnitude of the clutter power, as expressed by the normalized radar cross section  $\sigma_0$  introduced by Goldstein (1). The parameter  $\sigma_0$  is a dimensionless quantity, which may be made relatively independent of the measuring system. To date, many measurements of  $\sigma_0$  or an equivalent quantity have been made with various radar systems over a wide range of sea conditions (2). A study of the literature will show that, despite extensive investigations, comparisons of  $\sigma_0$  values obtained from different experimenters result in inconsistencies. These inconsistencies are mainly the result of difficulties involved in the comparison of data taken with different systems and calibration techniques for different surface conditions.

In the past, sea-clutter data have been obtained at various radar wavelengths by using individual radar systems, each requiring a separate calibration. Furthermore, each system has employed a specific sampling and integrating device (e. g., a range gate of fixed width or an automatic gain control (AGC) loop) and recorded its output by various means (e. g., film, strip chart, or magnetic tape). The combined effect of the sampling-integrating-recording procedure on the power return differs considerably among various systems. Thus, "mean" values of  $\sigma_0$  obtained from one system may not necessarily be directly comparable to "mean" values obtained from another (3).

The specification of the sea surface is also a formidable problem. Sea clutter is generally a function of surface wind velocity and wave height, which are both time-dependent variables. The specification of these variables, even as gross averages, requires considerable effort, particularly in the case of an airborne radar measurement over the open sea. Since wind velocity is subject to radical changes within a relatively short period of time, it is important to obtain a record of its variation during a radar recording period. On site estimates of the prevailing winds and wave heights during a clutter measurement are a minimum requirement in regard to surface specification. This information is necessary to insure that clutter data taken at different times do indeed apply to similar sea-surface conditions. An experiment designed to measure the effect of incident angle, radar wavelength, and polarization on the value of  $\sigma_0$  must also specify the gross surface conditions during the operating period.

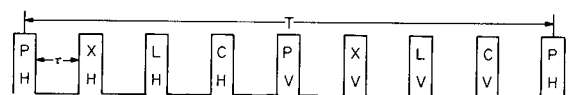
From July 13, 1965, to July 29, 1965, NRL, in conjunction with the Applied Physics Laboratory (APL) of Johns Hopkins University, conducted an extensive sea-clutter measurement program off the coast of Puerto Rico. This location was selected to obtain data for a wide variety of sea conditions. It is believed that this experiment succeeded in monitoring the factors discussed above to a greater extent than any previous experiment performed by NRL. The NRL WV-2 instrumented aircraft and the vessel Peacock instrumented by APL were used in this experiment. The NRL 4FR system operates on four frequencies and alternate vertical and horizontal polarization. A

common receiving system for each polarization provides virtually simultaneous data on four wavelengths, which are calibrated in flight. A high sampling rate coupled with magnetic tape recording produces a permanent pulse-to-pulse record of the sea return. Later, effective integration is accomplished through in-house digital computer facilities. The experiment was conducted in the following manner: While the airborne radar recorded sea clutter over an area marked by the position of the oceanographic vessel, the APL group gathered sea-surface data in the form of stereophotographs, wave-buoy measurements, and wind-velocity readings. The vessel was used as one terminal of the aircraft flight path to provide a reference for the radar data. The radar data could then be correlated with the daily gross variations of local wind velocity and wave height. In addition to the gross measurements, APL obtained fine-structure surface information in the form of ocean wave spectra and wave profiles (4, 5). Theoretical work on the measurement of ocean wave spectra by a holographic technique is also continuing at NRL (6, 7).

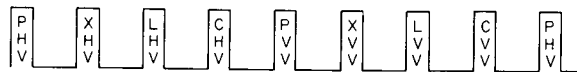
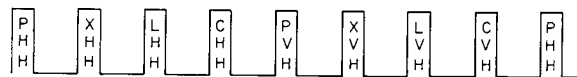
The sea-surface data collected by APL enabled compilations to be made which compare the values of  $\sigma_0$  obtained at different polarizations, radar wavelengths, and incident angles for equivalent sea conditions. The correlation of the NRL radar results with the ground truth obtained by APL provides a large bank of information on the behavior of the normalized radar cross section  $\sigma_0$  from which both the radar designer and the oceanographer may work.

#### INSTRUMENTATION

The 4FR pulsed radar and its antenna system have been described in previous reports (8, 9), so that only a brief description need be given here. The system transmits in the sequence P band (428 MHz), X band (8910 MHz), L band (1228 MHz), and C band (4455 MHz), alternately on vertical and horizontal polarization, receiving both the vertical and horizontal component of the return. The transmission and reception sequences are diagrammed in Fig. 1, where T equals the basic repetition period. It is seen that a total of 16 signal amplitude components are recorded - eight on direct polarizations and eight on the cross polarizations. The labeling convention as shown in Fig. 1 ( $P_{HH}$ , etc.) will be adhered to in this report.



4FR TRANSMISSION SEQUENCE



4FR RECEPTION SEQUENCE

Fig. 1 - Pulse train

A simplified block diagram of the receiving system is shown in Fig. 2. The receiving system consists of four i-f amplifiers (37 MHz) through which all the radars are multiplexed on a time-share basis. Two of the amplifiers are fed by the horizontally polarized signal, and two are fed by the vertically polarized signal. One of these is a logarithmic strip whose output is detected square law and provides a pulse-to-pulse measure of the amplitude in the range gate. The second of these is a linear strip whose output is hard clipped to eliminate amplitude fluctuations and provides a measure of instantaneous signal phase. A similar log-lin pair of receivers exists for the vertically polarized returns. The output of each detector is range gated, digitally quantized to 128 levels (seven bits) and recorded on magnetic tape at the pulse repetition rate. Formatting circuitry separates the various frequency and polarization combinations and assigns to each a definite position to allow later identification.

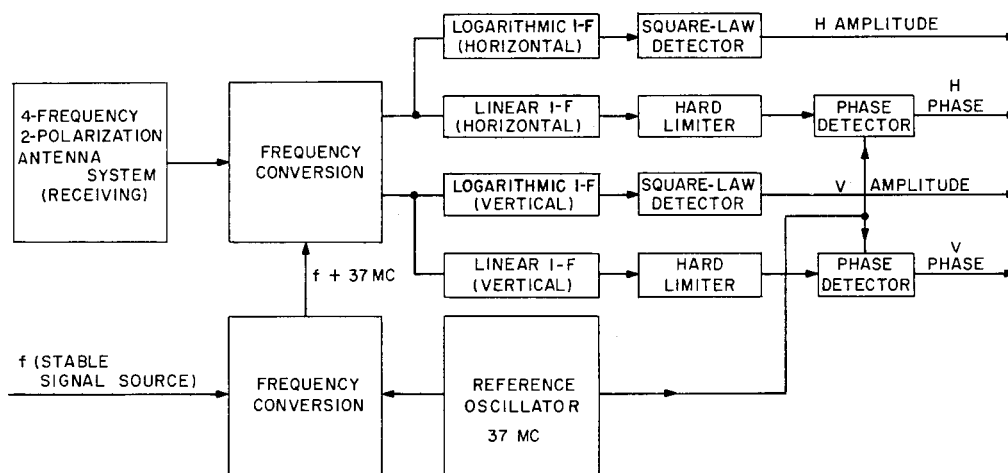


Fig. 2 - Four-frequency receiving system

The system also features common antennas pointing through 100 degrees of elevation. The X-band and C-band antennas are parabolas mounted side by side in the radome on the underside of the aircraft. This pair is mounted back to back with the P-band and L-band crossed dipole antennas. Both antenna pairs are colinear, so that the X and C band illuminate the same area, and, likewise, the P and L band illuminate the same area, although the P-band beam is larger and actually includes the area illuminated by the L-band beam. The antennas are stabilized in roll and pitch and can sector scan through 315 degrees of azimuth and can turn through 100 degrees of elevation. The electrical characteristics of the antenna and the principal parameters of the radar system are given in Table 1. The 4FR system allows many choices of prf, pulse length, i-f bandwidth, range-gate width, and antenna angle. The values used for these parameters during the July program were prf, 788 pps; pulse length, 0.25  $\mu$ sec; i-f bandwidth, 10 MHz; range gate width, 50 nsec; antenna elevation angle, 4 to 9 degrees (vertical incidence); and antenna azimuth angle, 0 to 180 degrees.

The received clutter power is absolutely calibrated by referencing it to the power returned from aluminum spheres dropped from the aircraft. The spheres are dropped singly and manually tracked by the radar. Good estimates of the sphere cross section are obtained by recording the backscatter from several spheres for each wavelength. Since the antenna pairs are concentric, the X-band and C-band wavelengths are calibrated simultaneously, and, likewise, the L-band and P-band wavelengths are calibrated

Table 1  
 Four-Frequency Radar System Parameters  
 (Peak power - 20 to 40 kW, average power - 100 to 160 W, pulse width - 0.25 to 2.0 sec, prf. - 100 to 1463 pps)

Band	Azimuth Beamwidth (degrees)		Elevation Beamwidth (degrees)		Azimuth Minor Lobe (dB)		Elevation Minor Lobe (dB)		Cross Polarization (dB)		Antenna Gain (dB)	
	Horiz.	Vert.	Horiz.	Vert.	Horiz.	Vert.	Horiz.	Vert.	Horiz.	Vert.	Horiz.	Vert.
P	±12.3	12.1	40	41	14.5	14.5	30	26.0	25	28	17.4	17.4
L	5.5	5.5	13.8	13	13.4	14	16	14	25	25	25.9	26.2
C	5	5	5	5	23.2	23.2	24.5	24.5	>20	>20	31.4	31.4
X	5	4.7	5.3	5.0	23.6	23.6	23.5	24.2	>20	>20	31.2	31.2

simultaneously. Applying the usual radar equation to the sphere signal (1), where the subscript S denotes the sphere measurement, gives

$$\sigma_S = \frac{(4\pi)^3 P_{RS}}{G^2 \lambda^2 P_{TS}} R_S^4. \quad (1)$$

In the case of sea clutter, the normalized radar cross section is defined by

$$\sigma_0 = \frac{\sigma}{A}, \quad (2)$$

where A is the illuminated area. Then the radar equation for clutter becomes

$$\sigma_0 = \frac{(4\pi)^3 P_R}{G^2 \lambda^2 P_T} R^4 A. \quad (3)$$

The ratio of Eq. 3 to Eq. 2 yields

$$\sigma_0 = \frac{P_R}{P_{RS}} \frac{R^4}{R_S^4} \sigma_S A, \quad (4)$$

where the peak power transmitted is the same for both measurements. From Eq. 4 the value of  $\sigma_0$  is easily calculated for a recorded value of received power  $P_R$  at a known range R. The sphere terms in Eq. 4 are determined by the in-flight measurement, and the illuminated area A is calculated from the geometry of the data run. At small incident angles the area is pulse-length limited and is approximated by

$$A = R \phi_a \frac{1}{2} CT / \cos \theta, \quad (5)$$

where  $\phi_a$  is the azimuth beamwidth between half power points, T is the pulse length, and  $\theta$  the incident angle. At large angles when the area is beamwidth limited, it is approximated by

$$A = R^2 \phi_a \phi_e / \sin \theta, \quad (6)$$

where  $\phi_e$  is the elevation beamwidth between half-power points.

#### DATA COLLECTION AND PROCESSING

A characteristic property of sea clutter is the variation of the radar cross section RCS with the incident angle. To measure this variation, the following flight plan was used. The aircraft maintained a steady course in alternate upwind, downwind, and cross-wind directions, using the surface vessel employed by the APL group as a marker to insure that radar data were collected from the area of oceanographic measurement. The antenna pairs were set at azimuths of 0 and 180 degrees, respectively, and the desired elevation angle. When the appropriate aircraft heading was attained, with respect to the Peacock, data recording commenced. The geometry of a typical recording is illustrated in Fig. 3. Generally, recording was done at three or four different elevation

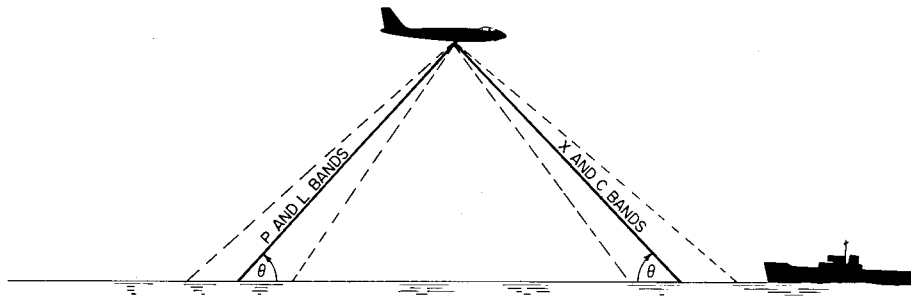


Fig. 3 - Geometry of a fired-angle run

angles during one run for about 30 seconds per angle. Thus, it was possible to collect a representative sampling of clutter at various incident angles from near grazing (4 degrees) to normal incidence (90 degrees) in the upwind, downwind, and crosswind directions efficiently.

Since radar clutter is a statistical process, the random return is best described by its probability distribution. The calculation of the distribution is accomplished through the use of a general purpose digital computer with magnetic tape input and plotter output. The basic outputs of the processing system are plots of received power (in decibels) versus time, in terms of the 10%, 50% (median), and 90% percentiles of successive cumulative probability distributions. A typical plot is illustrated in Fig. 4, for one ( $X_{VV}$ ) of the 16 amplitude components ordinarily recorded during each run. The data are initially plotted against an arbitrary decibel scale on the left. This scale is calibrated by the sphere measurement to provide the values of normalized cross section  $\sigma_0$ . The return is referenced to the oceanographic data, since the position of the Peacock is marked by the sharp increase in signal toward the end of the run. To study  $\sigma_0$  as a function of other parameters, the median value of  $\sigma_0$  was determined from plots, such as Fig. 4, through the region of interest, usually near the surface vessel. These values were tabulated on all frequencies and polarizations for each data run, and the median value of  $\sigma_0$  observed over a 20- to 30-second time interval. Over 200 data runs were recorded during the July 1965 period, with from one to six angle settings per run. With 16 signal amplitude components available for processing, a vast amount of data has been generated. To keep this report within manageable proportions, only data on the direct polarizations (i. e., VV and HH) will be presented below. Cross-polarized results will be presented in a later report.

## DATA PRESENTATION

The study of these data revealed the expected variation in  $\sigma_0$  with wind direction at moderate angles, as well as run-to-run differences for  $\sigma_0$  in the same direction. While small run-to-run differences may be attributed to receiver stability, larger effects were due to the nonstationary nature of the sea surface. In particular, the short wavelengths (X and C bands) were most sensitive to upwind-downwind-crosswind relations and to short-term fluctuations in the wind velocity. To minimize these effects, the runs in the upwind direction were selected and the value of  $\sigma_0$  tabulated, when available, at each angle. These values were those most closely associated with the gross surface conditions observed for any particular day. From the point of view of a radar designer, the data to follow provide the most conservative (worst case) estimates of sea clutter for the stated surface conditions. These conditions are gross estimates of wind velocity and wave height made by observers aboard the Peacock at various intervals throughout the day. The estimates are listed in Table 2 for the July 1965 flights in an order approximating decreasing roughness. The scale ranges from

Table 2

Date	Location	Wind Velocity (knots)	Wave Height (feet)	Angles Sampled (degrees)	Qualitative Observations
July 15, 1965	10 mi N. W. San Juan	15-20 10-15	4-5 3-5	4-20 30-90	Rain Rain
July 19, 1965	15 mi N. W. San Juan	10-12 10-15	3-4 3-4	4-45 70-90	
July 23, 1965	20 mi N. W. San Juan	8-10 8-12	2-3 4-6	30-60 4-20, 70-90	Sea "choppy" white caps
July 22, 1965	20 mi N. W. San Juan	10-12 10-12	5-7 3-4	4-60 70-90	5-8-ft swells
July 16, 1965	10 mi N. W. San Juan	10-12 7-8 8-10 15-18	2-2.5 2-3 3-4 3-4	4-15 20, 30 45-90 80	Rain squall
July 21, 1965	20 mi N. W. San Juan	8-11  8-11	4-6  3-5	4 in X and C; 10 in L and P 10-90	Gusts to 12 knots
July 20, 1965	15 mi N. W. San Juan	7-9 10-12 10-12	2-3 2-3 2-3	5-45 60-90 4 (cross- wind only)	
July 29, 1965	off Mayaguez	1-2 1-2 2-15	1-2 1-2 2-3	60-90 20-60 4-60	White caps
July 27, 1965	off Mayaguez	2-3 5-8 0-1	0.5-1 1-2 and 4-5 0.5-1	4-15 15-66 60-90	"Confused" sea-squall
July 28, 1965	off Mayaguez	0-1 3-4	0.5-1 0.5-1	4-18, 60-90 4, 34	2-ft swells Rain squall
July 27, 1965	off Mayaguez	2-3 0-1	0.5-1 0.5-1	4-20 60-90	Natural slicks
Dec 9, 1964	50 mi east of Atlantic City,	12-15	6-10	3-90	Well- developed sea
Dec 10, 1964	N. J.	4	2-4	5-90	Natural slicks

moderately rough conditions of up to 20-knot winds and 5- to 7-foot wave heights to natural slick conditions observable on July 27, 1965. Also included in Table 2 are references to December 1964 data published previously (10). Some of those results are also included below.

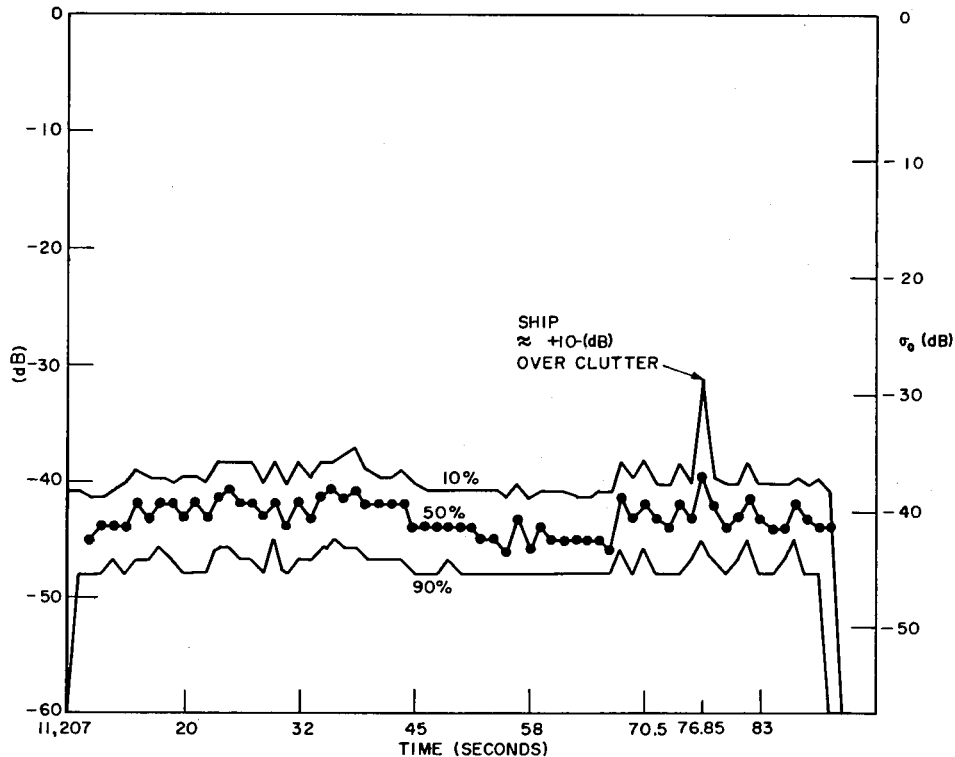


Fig. 4 - Sample median plot. Run 170 was made on July 29, 1965 with  $\theta = 20$  degrees, polarization = VV, and frequency = X.

As is well known, the behavior of  $\sigma_0$  with the angle generally depends on the angular region in question. Early investigations showed that at small angles there is a "critical" angle below which  $\sigma_0$  decreases rapidly with the angle. At angles higher than the critical angle,  $\sigma_0$  increases slowly until a high angle region is reached, after which  $\sigma_0$  increases rapidly to its maximum value at 90 degrees. The three angular domains may simply be called the low-, medium-, and high-angle regions or, more usually, the interference, plateau, and specular regions, indicating the physical phenomena present. Katzin (11) explained the existence of the critical angle in terms of interference between the direct and reflected ray from the surface-scattering element. From the interference mechanism he deduced that the critical angle is a function of polarization and that it increases with radar wavelength and decreases as sea roughness increases (2). To explain the plateau-region behavior of  $\sigma_0$ , Katzin hypothesized the existence of scattering elements or "facets." The wavelength dependence of  $\sigma_0$  is then determined by the size distribution of the facets, and the angular variation of  $\sigma_0$  is determined by the slope distribution of the facets. This model accounts for scattering in the three angular regions and predicts the same frequency dependence of  $\sigma_0$  at high angles as at low angles.

More recently, the slightly rough scattering theory formulated by Rice (12) has been applied to a sea-clutter model. In this theory, the scattering elements are surface irregularities which are small compared to the radar wavelength. Peake (13) applied the theory to the electromagnetic backscatter case, and Wright (14) developed a rough

surface model in which the scattering elements are slightly rough particles of water riding on longer gravity waves. Predictions based on this model have resulted in good agreement with measured values of  $\sigma_0$  for vertical polarization. Valenzuela (15) extended the theory to second order to show how the tilt of the rough patches with respect to normal incidences produces polarization effects. The slightly rough theory directly relates the radar return to the energy spectra of the surface. The predicted wavelength dependence of  $\sigma_0$  will then depend on the form of this spectrum.

#### DEPENDENCE OF $\sigma_0$ ON INCIDENT ANGLE

In accordance with the introduction outlined above, curves of  $\sigma_0$  versus incident angle for each surface condition encountered are given in Figs. 5 to 10 for all wavelengths. The curves are grouped by polarization and are presented in approximate order of decreasing sea roughness. Note that July 27, 1965, is given by two curves on each polarization. This is due to the presence on the surface of natural slick areas. With the help of the on-site oceanographic observations, it was possible to discriminate between two essentially different areas referred to on the plots (Figs. 7 and 10) as "rough" and "calm." The rougher area on July 27, 1965, is associated with the conditions listed in Table 2. The calmer area is a mixture of rough and calm patches on the surface.

The critical angle is not well defined by the curves because the clutter was sampled at discrete angles. However, some qualitative observations are possible. On vertical polarization, the critical angle is less than 10 degrees for all wavelengths and approximately independent of sea conditions. On horizontal polarization, the angle increases with increasing wavelength and occasionally vanishes for the P band on the calmer days.

It is also apparent in the long wavelengths that the critical angle increases with surface roughness. These results are in accord with what is expected on the basis of the interference phenomenon; further discussion may be found in the literature (2, 16).

In the specular region,  $\sigma_0$  increases rapidly with angle to its maximum at a 90-degree incidence. Comparison of the calm conditions with the rougher conditions shows the general tendency of  $\sigma_0$  at 90 degrees to decrease with increasing roughness. However, the trend is not uniform for each wavelength, as study of Figs. 5 to 10 will show. It has been suggested by Parks (17) that  $\sigma_0$  at vertical incidence may be a function of range, illuminated area, and antenna gain. It is believed that future NRL work will acquire more data at vertical incidence in the hope of verifying one of the existing models for the 90-degree case.

#### DEPENDENCE OF SEA CLUTTER ON SEA STATE

To estimate the effect of sea condition on the cross section  $\sigma_0$ , it is necessary to select surface parameters which will reflect increasing surface roughness. The gross measurements of wind velocity and wave height as given in Table 2 will be used as descriptors of the sea roughness. Figures 11 and 12 show  $\sigma_0$  as a function of average wind velocity and wave height for two angles (20 and 30 degrees) in the plateau region. For horizontal polarization, the more uniform increase of  $\sigma_0$  with wind rather than wave height indicates that this polarization is more sensitive to wind velocity. The plot  $\sigma_0$  versus wave height in Fig. 11 shows peaks which correspond to higher wind velocity. On vertical polarization, the return appears less sensitive to surface changes until calmer conditions are reached.

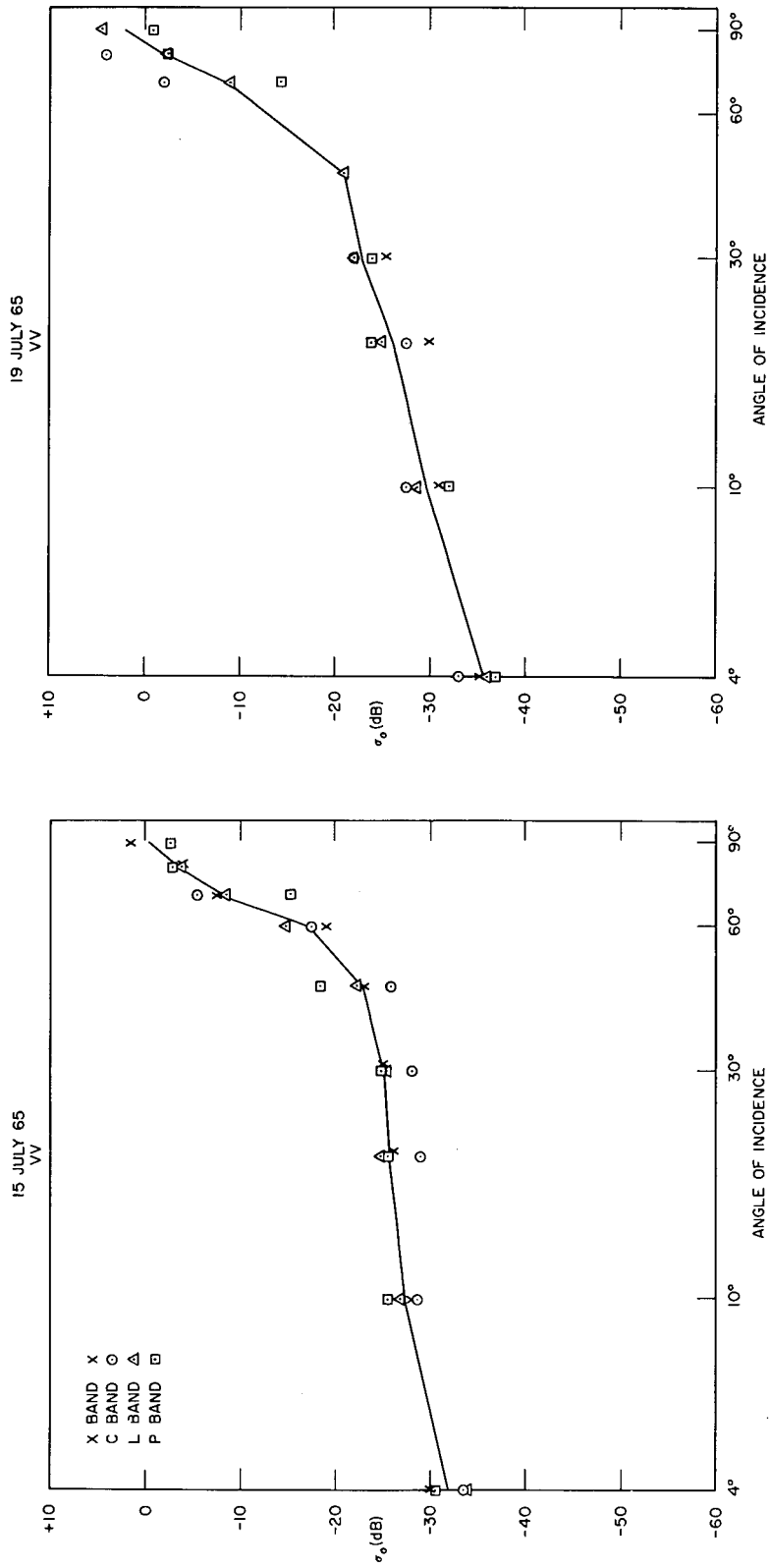


Fig. 5 -  $\sigma_0$  vs  $\theta$  for the four roughest conditions with a VV polarization

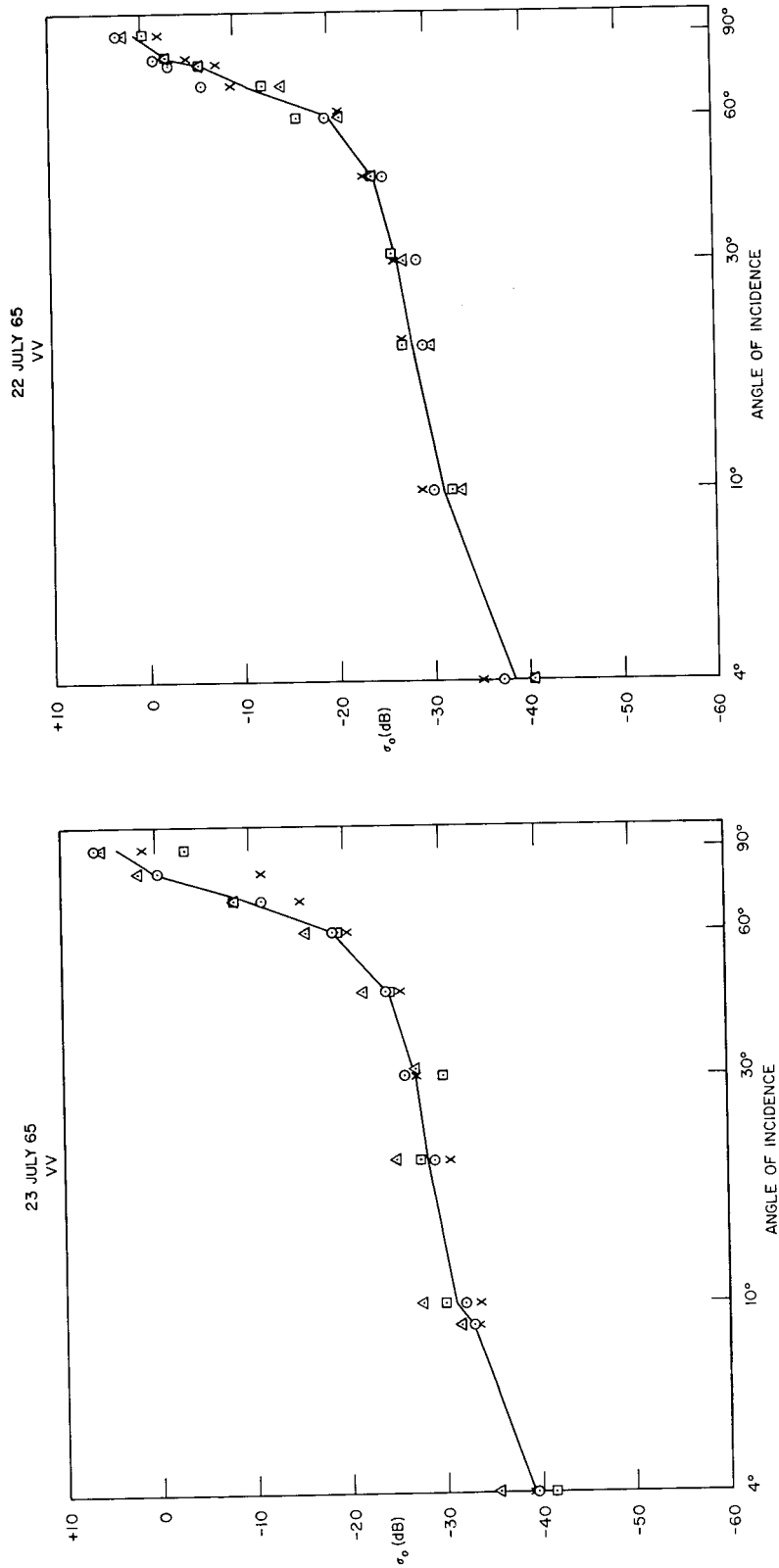


Fig. 5 (continued) -  $\sigma_0$  vs  $\theta$  for the four roughest conditions with a VV polarization

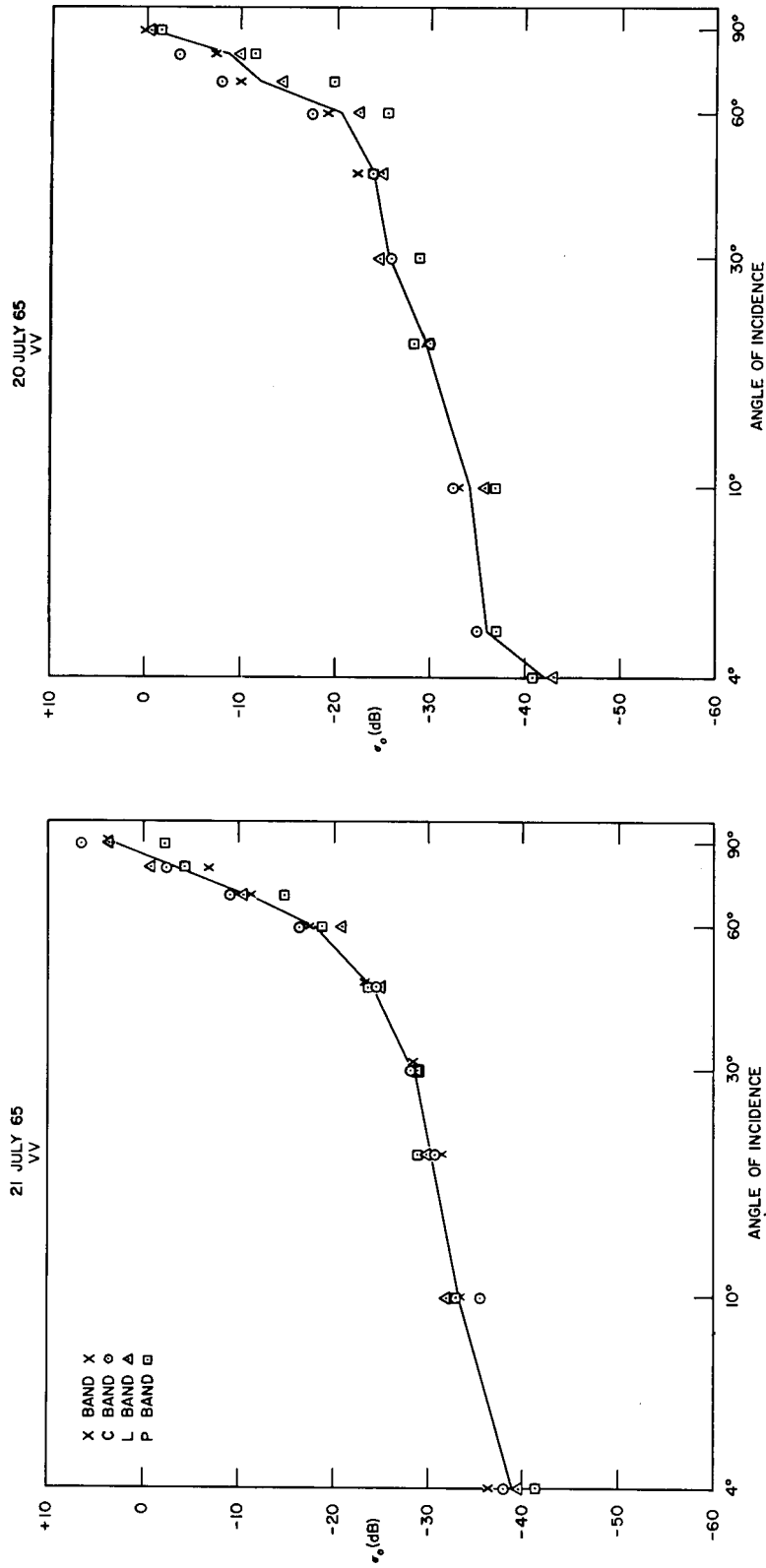


Fig. 6 -  $\sigma_0$  vs  $\theta$  for the next four roughest conditions with a VV polarization

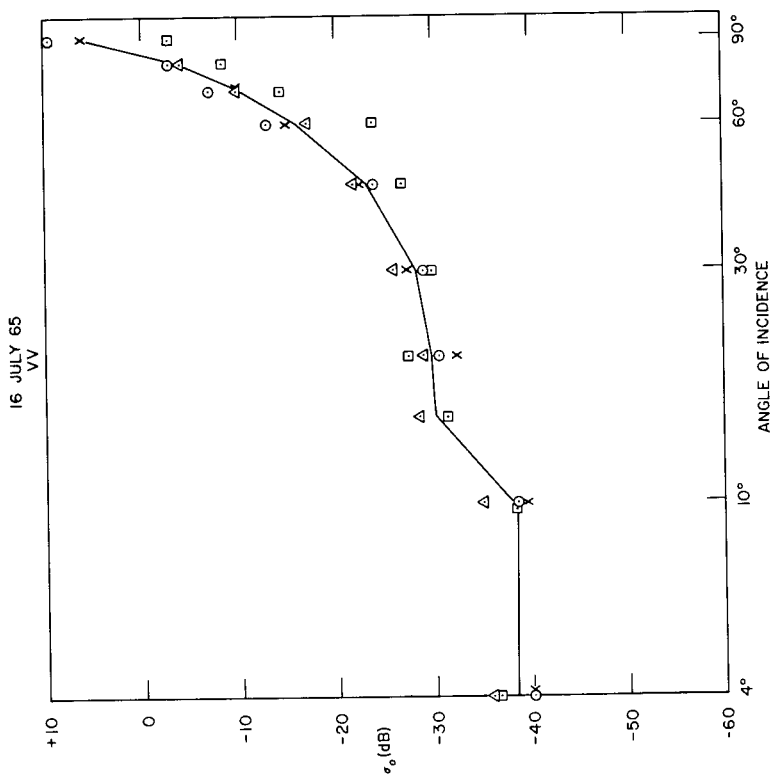
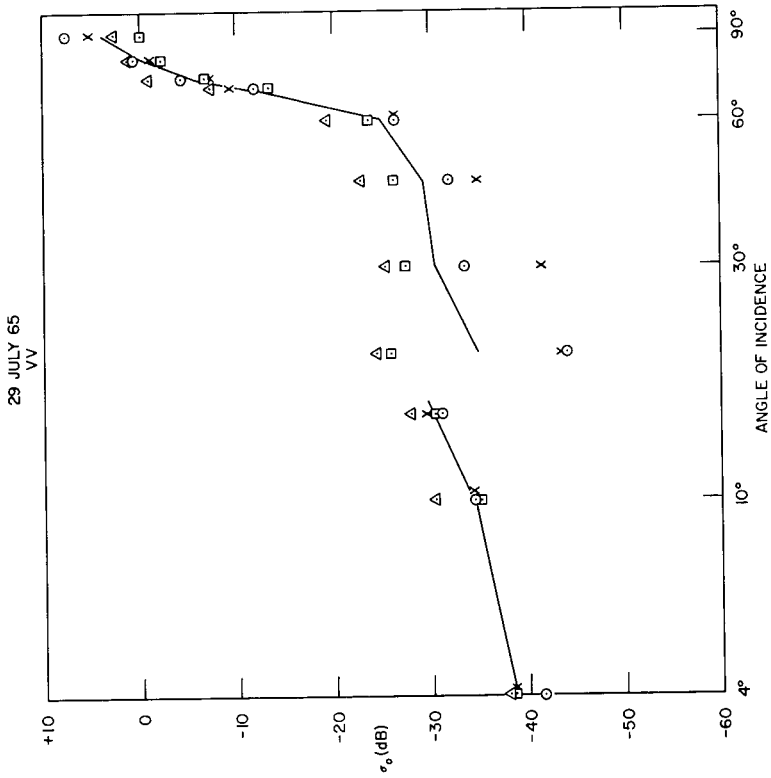


Fig. 6 (continued) -  $\sigma_0$  vs  $\theta$  for the next four roughest conditions with a VV polarization

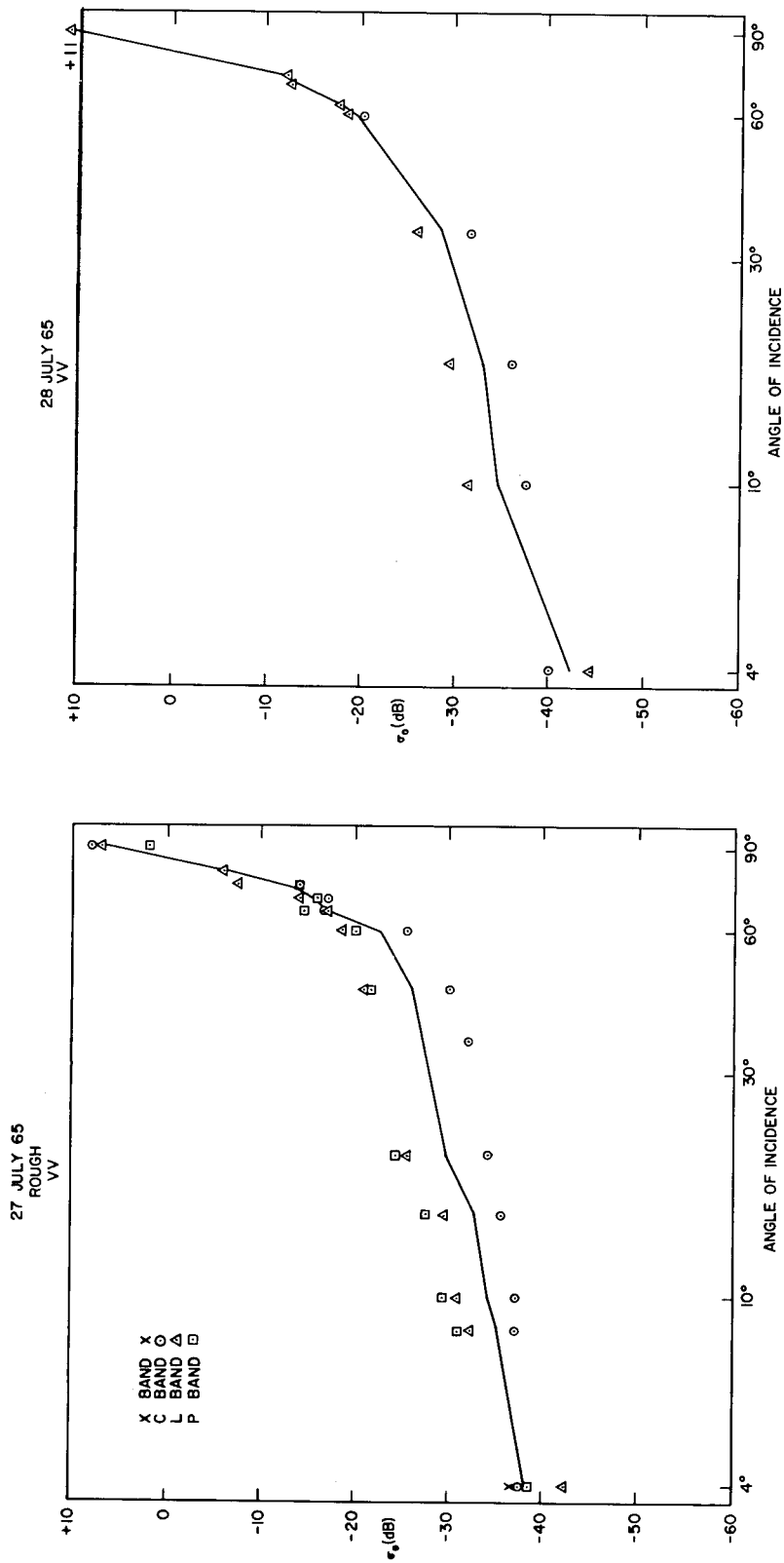


Fig. 7 -  $\sigma_0$  vs  $\theta$  for the calmer conditions with a VV polarization

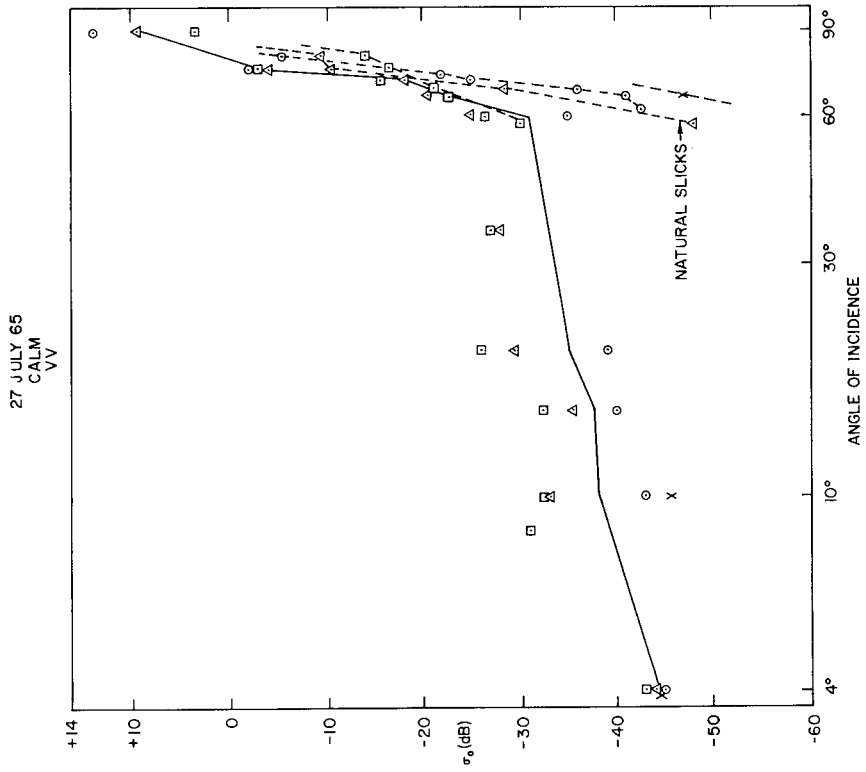


Fig. 7 (continued) -  $\sigma_0$  vs  $\theta$  for the calmer conditions with a VV polarization

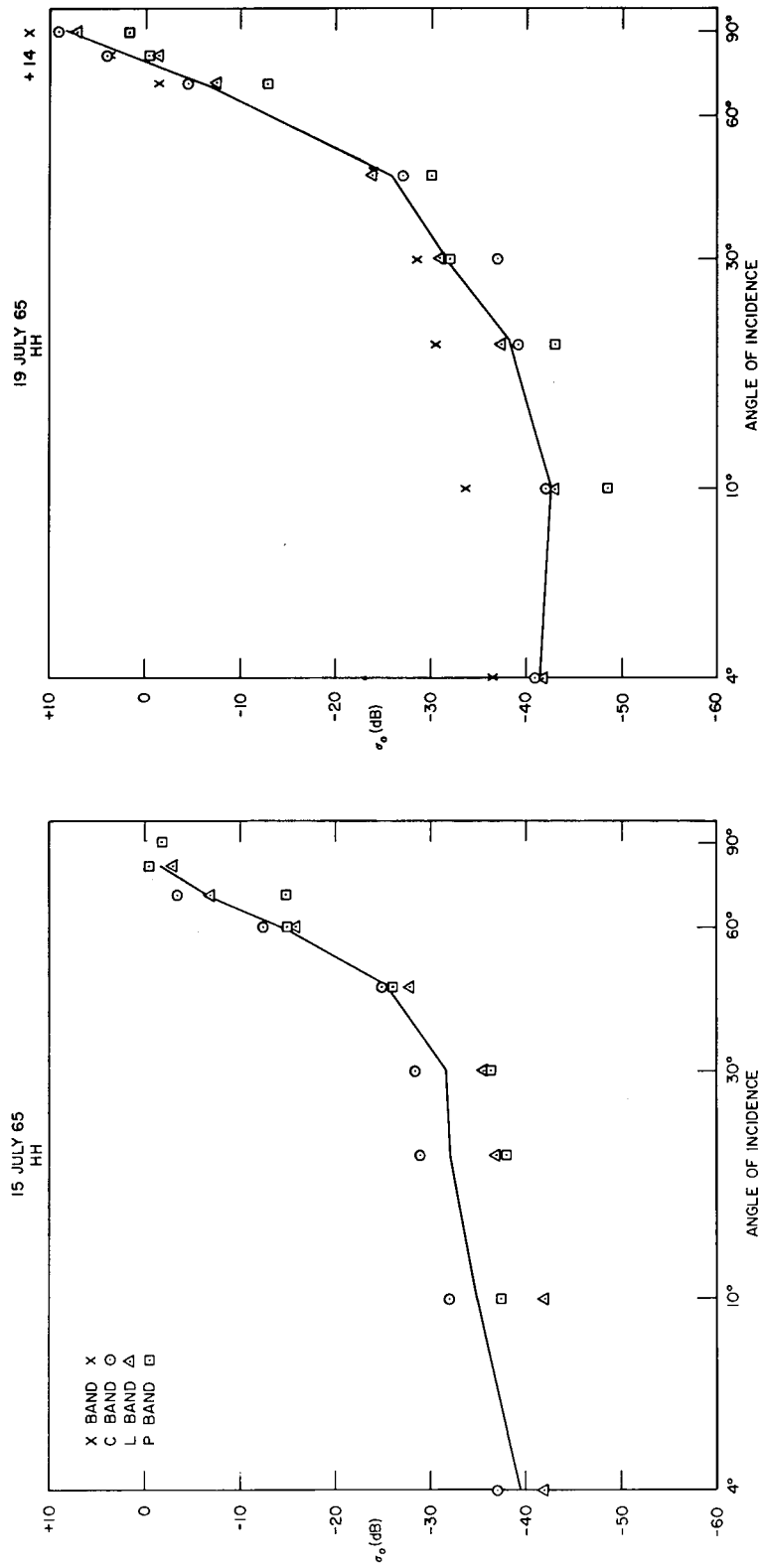


Fig. 8 -  $\sigma_0$  vs  $\theta$  for the four roughest conditions with an HH polarization

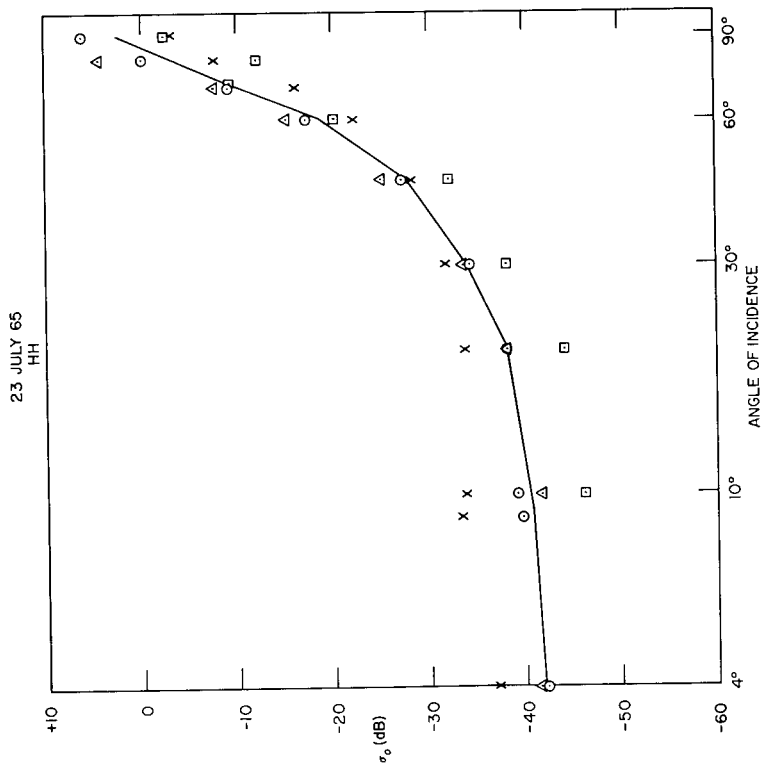
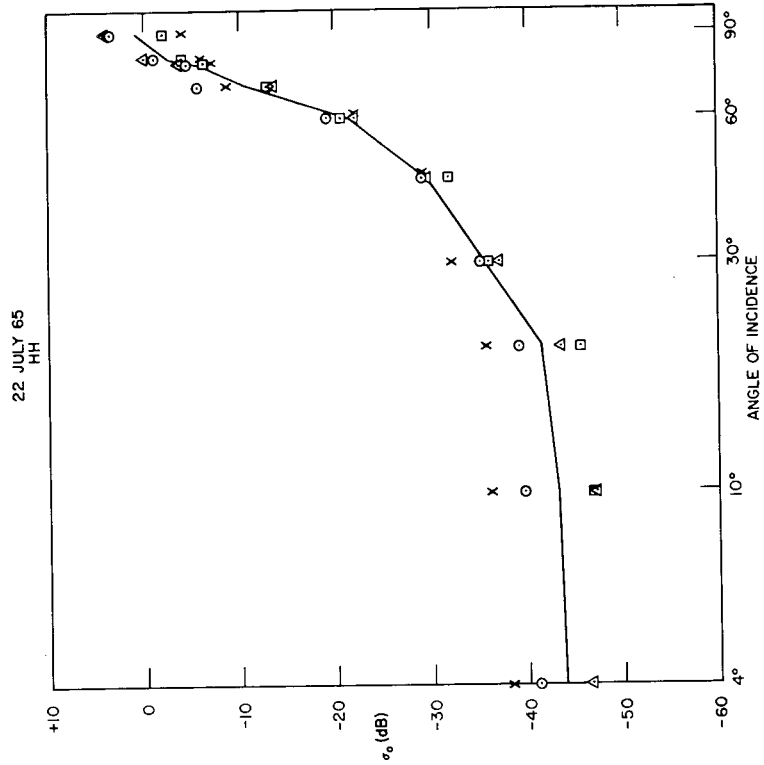


Fig. 8 (continued) -  $\sigma_0$  vs  $\theta$  for the four roughest conditions with an HH polarization

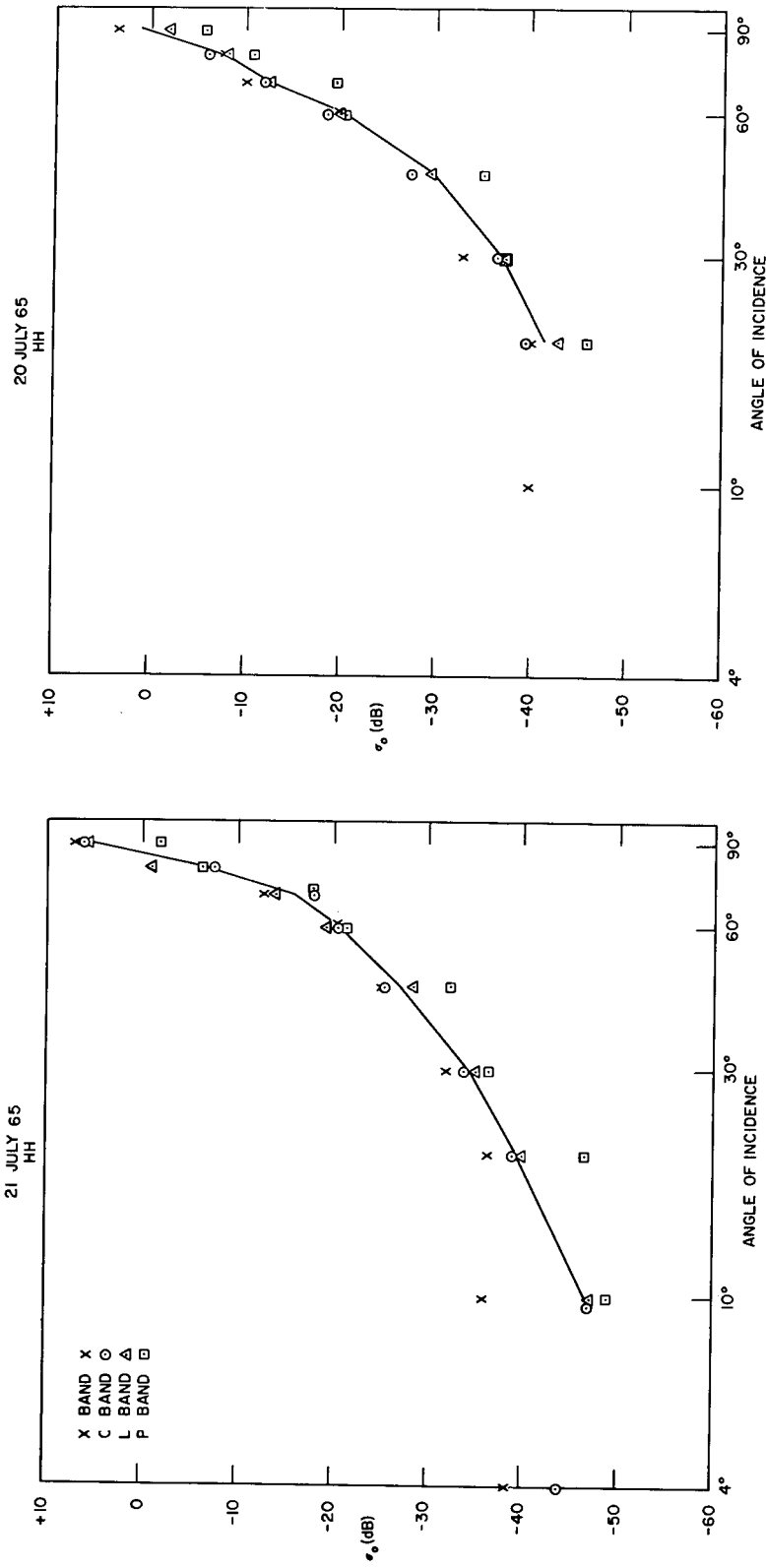


Fig. 9 -  $\sigma_0$  vs  $\theta$  for the next four roughest conditions with an HH polarization

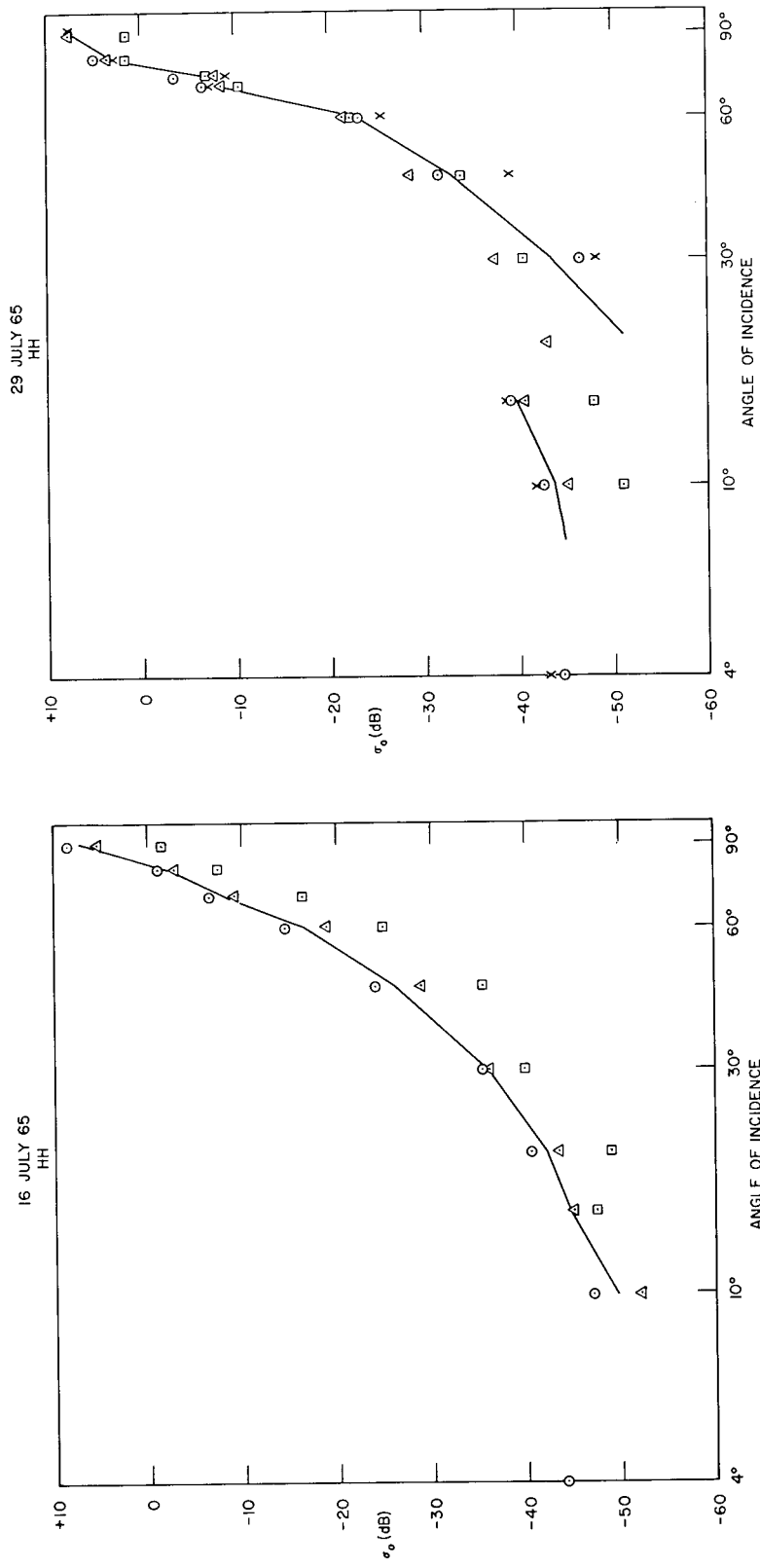


Fig. 9 (continued) -  $\sigma_0$  vs  $\theta$  for the next four roughest conditions with an HH polarization

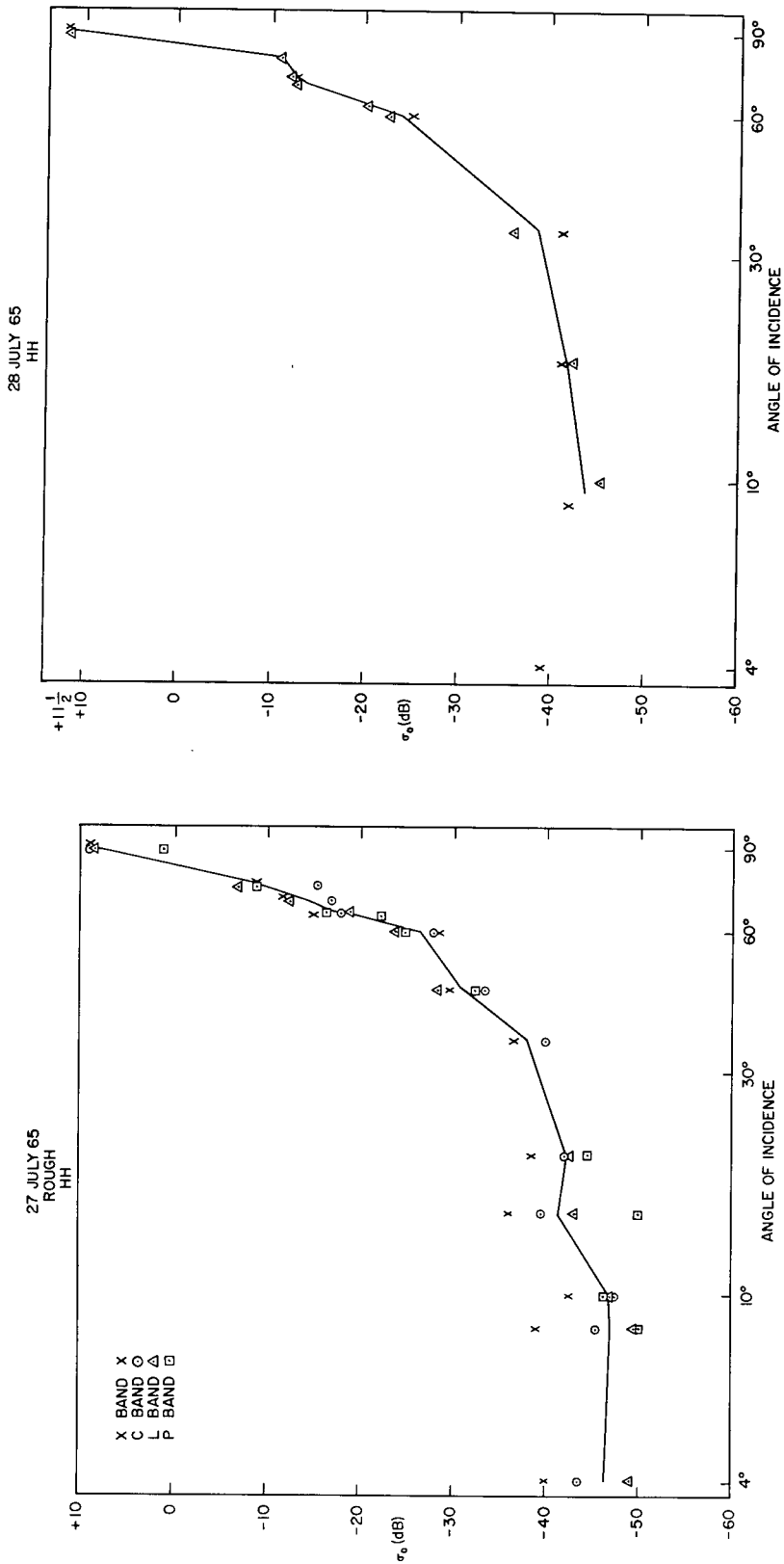


Fig. 10 -  $\sigma_0$  vs  $\theta$  for the calmer conditions with an HH polarization

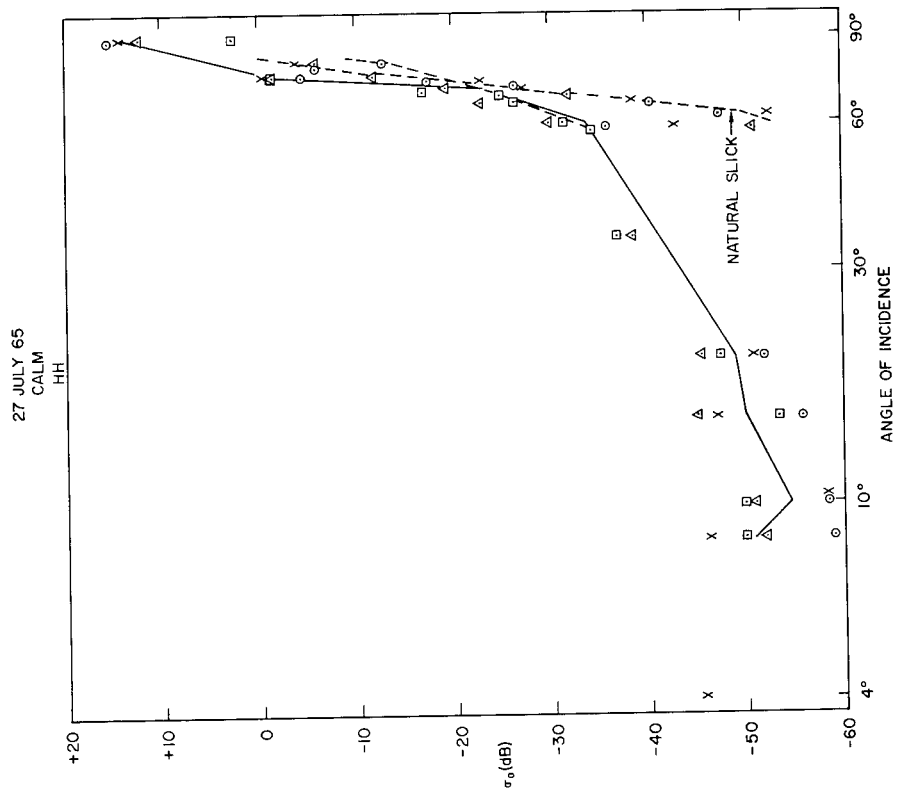


Fig. 10 (continued) -  $\sigma_0$  vs  $\theta$  for the calmer conditions with an HH polarization

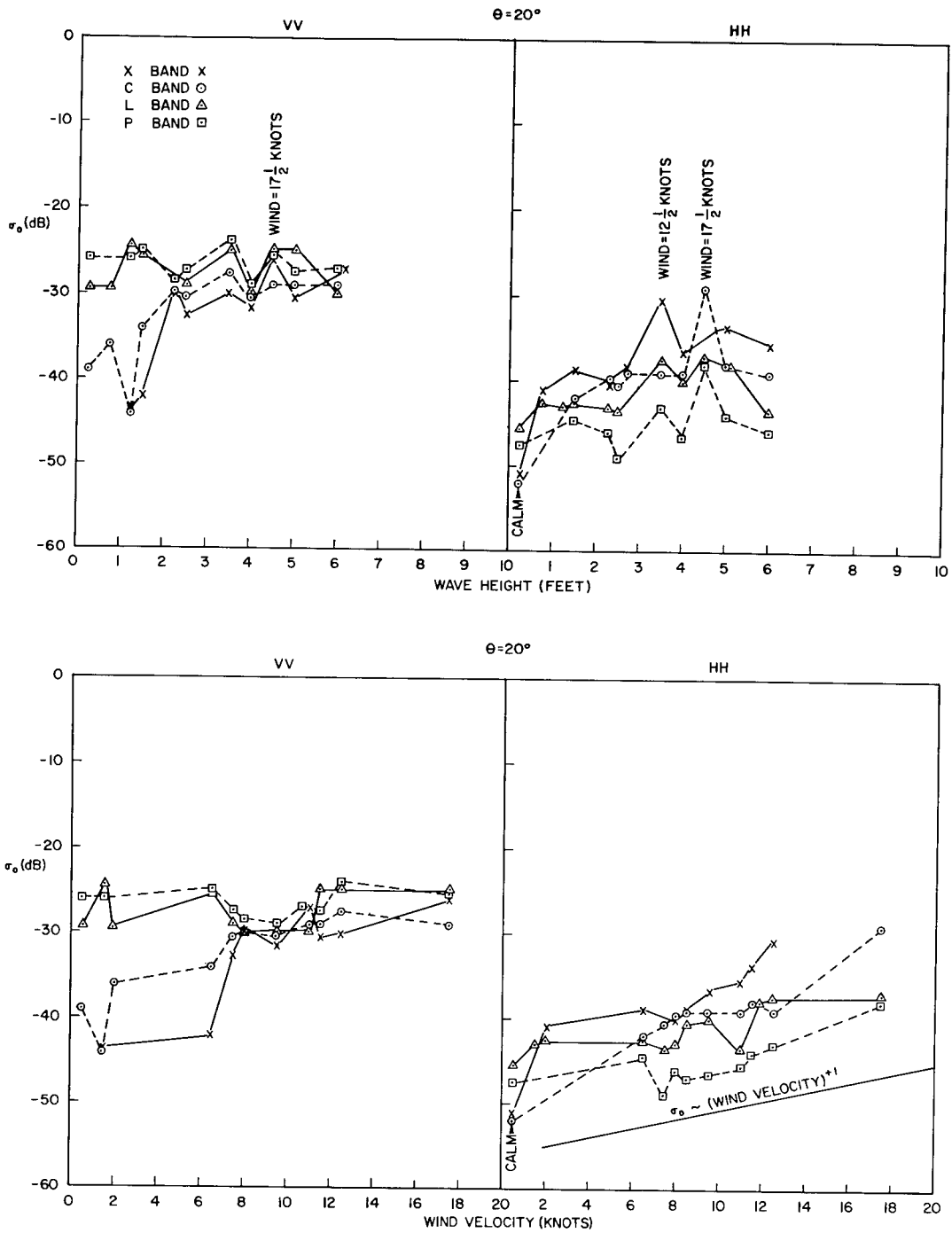


Fig. 11 -  $\sigma_0$  vs surface parameters for  $\theta = 20$  degrees

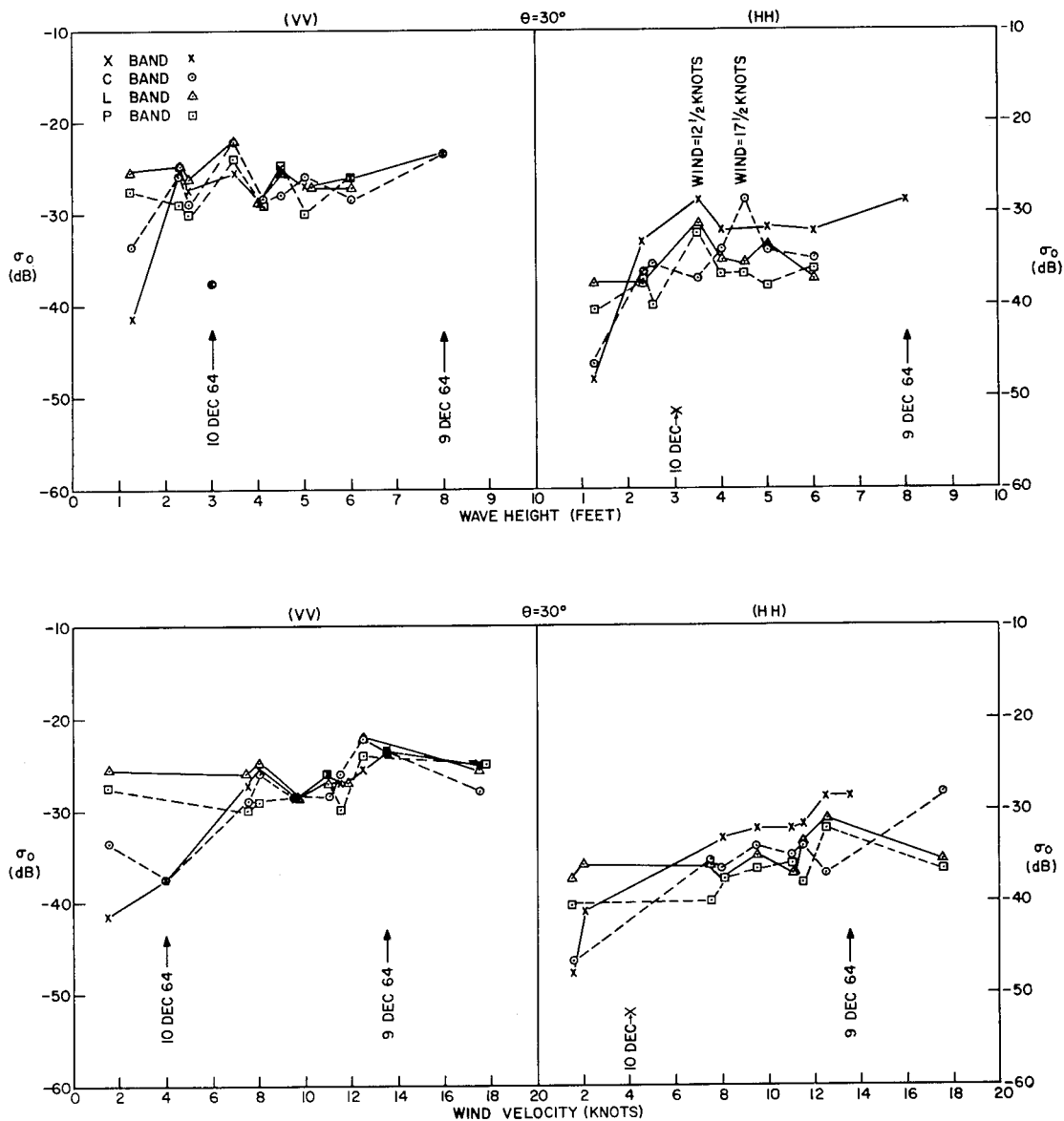


Fig. 12 -  $\sigma_0$  vs surface parameters for  $\theta = 30$  degrees

The wavelength dependence of  $\sigma_0$  appears to be a function of the polarization. On horizontal polarization the trend is approximated by  $\sigma_0(X) > \sigma_0(C) > \sigma_0(L) > \sigma_0(P)$ , while for vertical polarization this trend is absent. On vertical polarization the longer wavelengths produce a substantially larger return at calmer sea states.

#### DEPENDENCE OF SEA CLUTTER ON POLARIZATION

The relationship of  $\sigma_0$  to polarization is conveniently expressed by the direct polarization ratio  $\sigma_0(VV)/\sigma_0(HH)$  simply calculated in decibels by  $\sigma_0(VV) - \sigma_0(HH)$ . Figures 13 to 15 are plots of this parameter versus incident angle for each sea condition. The ratio is a function of incident angle, having a tendency to decrease at grazing and high-angle regions. It is also apparent that in the plateau region the polarization ratio is directly proportional to wavelength and inversely proportional to roughness. Figure 16 depicts this trend to polarization independence (0-dB ratio) as surface roughness increases. The downward trend on the X and C bands is seen to be more uniform as a function of wind velocity, indicating that this is the controlling factor for short wavelengths. The long wavelengths still show significant values for the roughest conditions encountered. For comparison purposes, a curve of VV/HH versus angle was computed for each wavelength representing the average of the four roughest days measured at Puerto Rico. Figure 17 gives this curve and compares it with data for rough and calmer conditions. This plot shows the decrease with surface roughness and a tendency to slightly negative values in the 70- to 90-degree region. In general, the data of Fig. 17 are in good agreement with past results (18, 19).

#### DEPENDENCE OF SEA CLUTTER ON WAVELENGTH

On vertical polarization, there is not a significant difference between wavelengths for the rougher sea conditions. To reduce the statistical scatter inherent in each measurement, averages of the  $\sigma_0$  versus angle curves were calculated for the four roughest conditions, the four next roughest conditions, and the four calmest conditions. The results are given in Figs. 18 and 19. The graphs in Fig. 18 clearly indicate that  $\sigma_0$  is independent of wavelength for vertical polarization in the plateau region for the two roughest sea conditions. The scatter between points is no more than would be expected due to wind variations. The calmest days, however, show smaller values of  $\sigma_0$  for the short wavelengths and reflect the presence of natural slick areas.

The corresponding averages for horizontal polarization are plotted in Fig. 19. A definite trend is observable on horizontal polarization, the short wavelengths being consistently higher in the plateau region. A median curve drawn through the plotted points effectively separates the X- and C-band values from the L- and P-band values. The plot of the calmer condition also indicates the critical-angle dependence, as L and P decrease more rapidly with angle and are no longer measurable at 4 degrees.

Included in Figs. 18 and 19 are the theoretical curves predicted from slightly rough scattering theory. The theory assumes a fully developed sea with a Phillips-Burling energy spectrum and provides good agreement with the vertically polarized return. A replot of the averaged  $\sigma_0$  in Figs. 18 and 19, as a function of angle in Fig. 20, shows that the wavelength dependence is maintained over the plateau and specular regions, a result predicted by the facet model.

Table 3  
Variation of Receiver Stability Level

Date	Receiver Variation (Stability) (dB)							
	X <sub>V</sub>	X <sub>H</sub>	C <sub>V</sub>	C <sub>H</sub>	L <sub>V</sub>	L <sub>H</sub>	P <sub>V</sub>	P <sub>H</sub>
July 15	±1	±1	±3	±1	±1	±0.5	±1.5	±1
July 16	±0.5	±0.5	±0.5	±0.5	±0.5	±0.5	±1.5	±1.5
July 19	±1	±0.5	±2	±1	±1	±1	±1	±1
July 20	±0.25	±0.25	±0.25	±0.25	±0.25	±0.25	±0.5	±2
July 21	±0.5	±0.5	±1	±0.5	±0.5	±0.5	±0.5	±0.5
July 22	±1	±0.5	±1	±0.25	±0.25	±0.5	±0.5	±1
July 23	±0.5	±0.5	±0.5	±0.5	±0.5	±0.5	±3	±0.5
July 27	±0.5	±0.5	±0.5	±1	±1	±0.5	±2	±2
July 28	—	±0.5	±0.5	—	±1	±0.25	—	—
July 29	±0.5	±0.5	±0.5	±0.5	±0.5	±0.5	±0.5	±0.5
Dec 9	±1	±1	±1	—	—	—	—	—
Dec 10	±1	±1	±1	—	—	—	—	—

#### SYSTEM LIMITATIONS

There are two basic errors in this measurement system: (a) receiver stability and (b) the measurement of the sphere. The receiver stability is monitored by recording an arbitrary reference level periodically through the day. The variation of this level is given (in decibels) in Table 3 for all components on each flight. The table shows that the receiving system is essentially steady. The sphere measurement possesses an uncertainty due to the variation of illumination of the sphere signal in the center of the beam. This uncertainty is minimized by recording several spheres on each frequency and is believed to be within 0 to 2 dB. When this uncertainty is combined with the statistical scatter of the sphere return around a range-4 slope, the result is an estimate of the limits of error of the sphere measurement (i.e., the absolute calibration). These estimates are listed for each component in Table 4.

However, the parameter under consideration determines which of the two basic errors (or both) are present. An absolute value of  $\sigma_0$  for a given component would involve both sources of error. However, a polarization ratio would essentially cancel the sphere uncertainty as would frequency ratios of L/P or X/C, since the sphere measurements are made simultaneously on each frequency pair. In view of the scatter inherent in any measurement of  $\sigma_0$  due simply to the nonstationary character of the sea surface, it is believed that the system accuracy represented in Tables 3 and 4 is sufficient to support the conclusions drawn in this report.

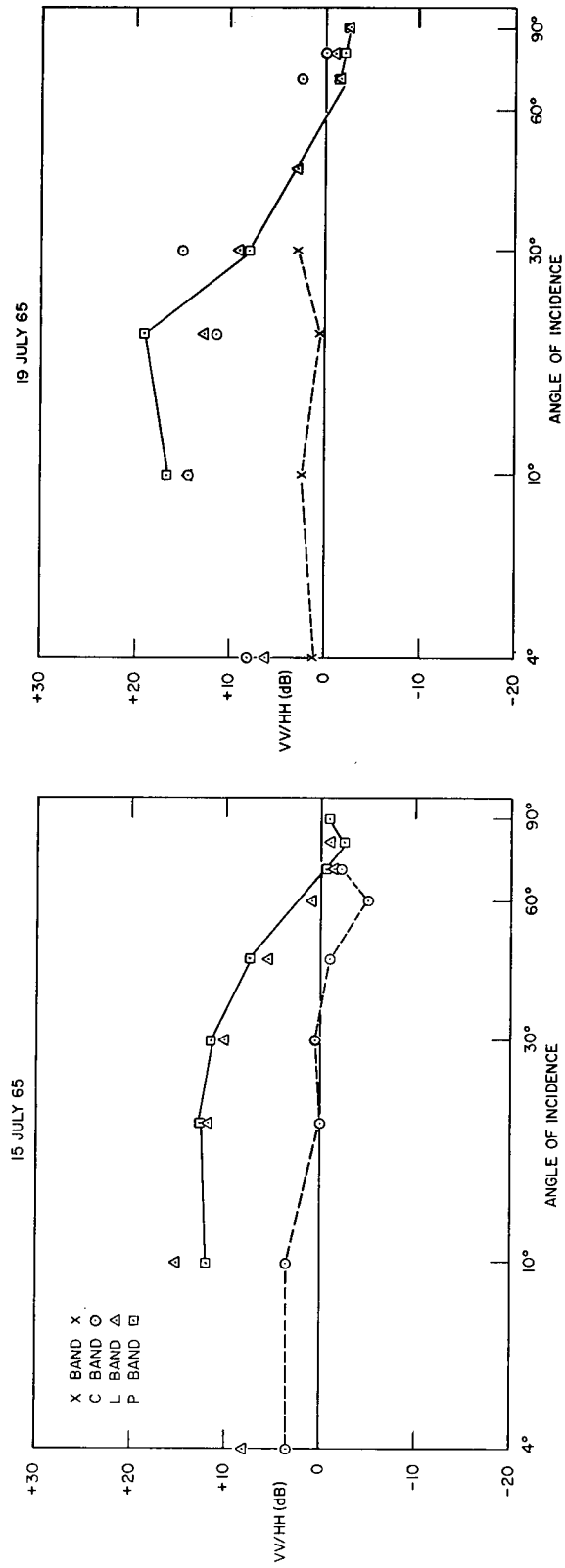


Fig. 13 - Polarization ratio (VV/HH) vs  $\sigma_0$  for the four roughest conditions

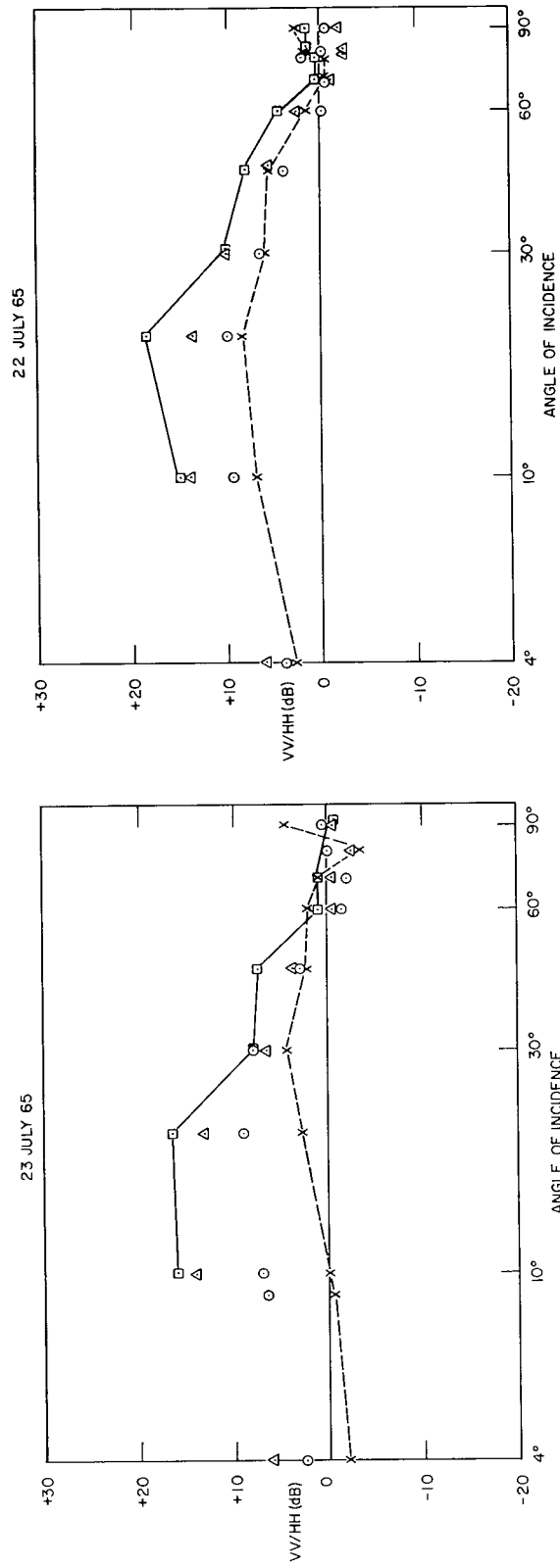


Fig. 13 (continued) - Polarization ratio (VV/HH) vs  $\sigma_0$  for the four roughest conditions

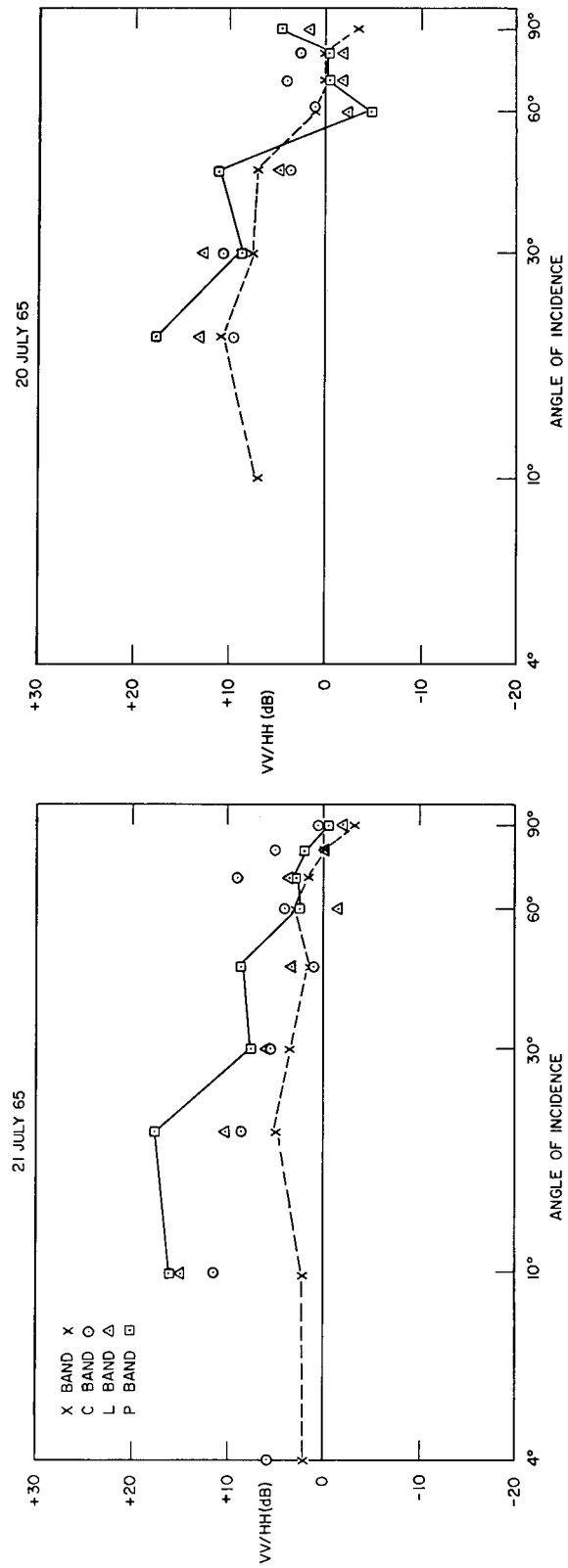


Fig. 14 - Polarization ratio ( $VV/HH$ ) vs  $\sigma_0$  for the next four roughest conditions

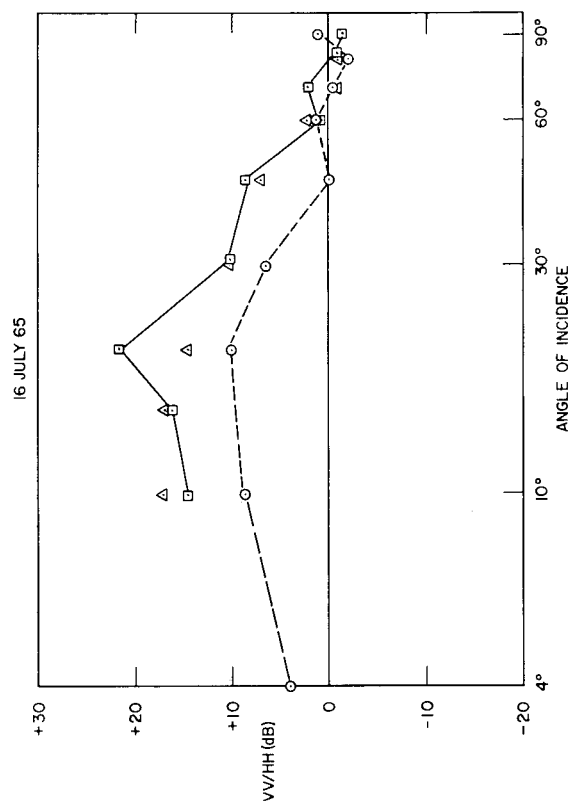
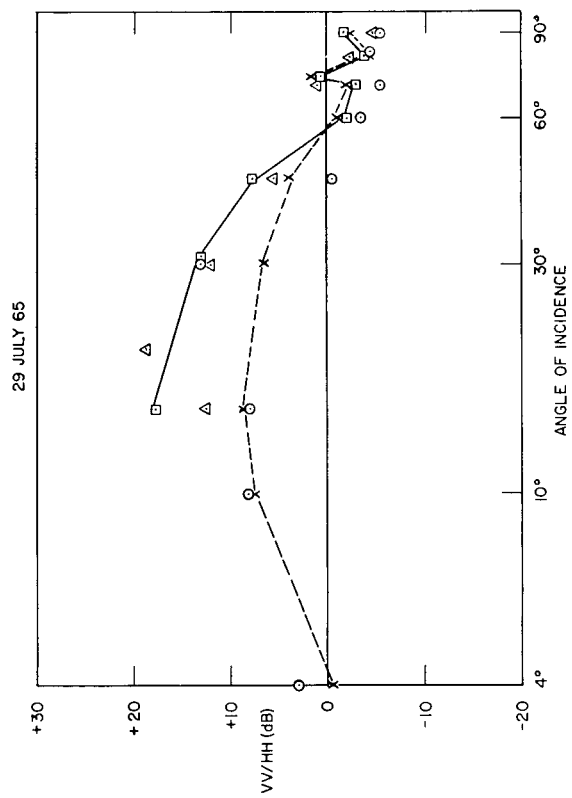


Fig. 14 (continued) - Polarization ratio (VV/HH) vs  $\sigma_0$  for the next four roughest conditions

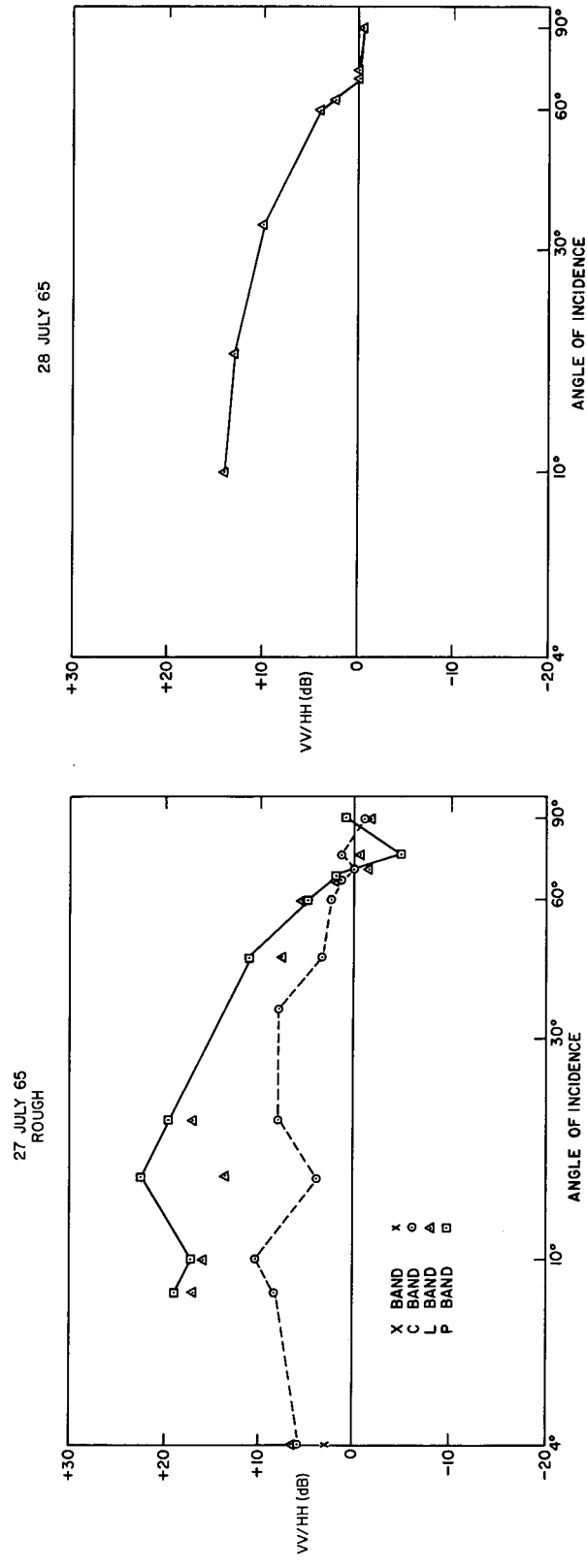


Fig. 15 - Polarization ratio (VV/HH) vs  $\sigma_0$  for the calmer conditions

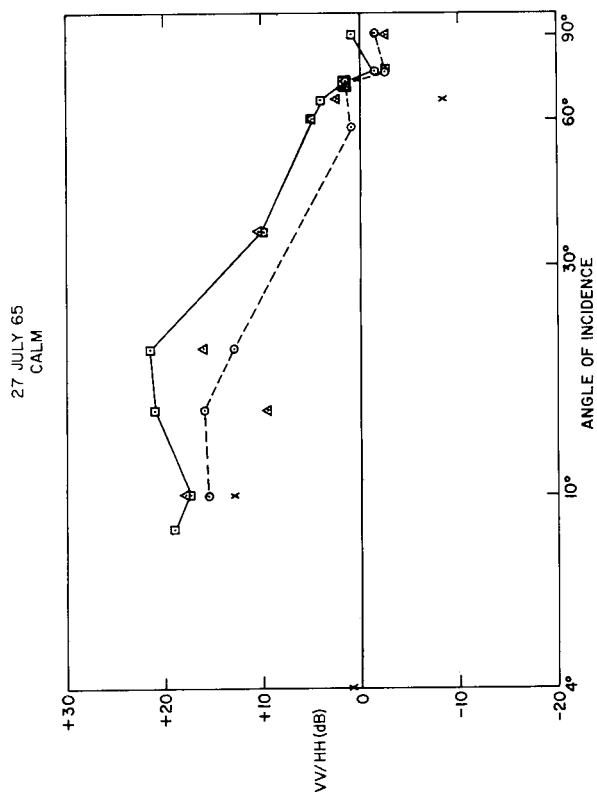


Fig. 15 (conditions) - Polarization ratio (VV/HH) vs  $\sigma_0$  for the calmer conditions

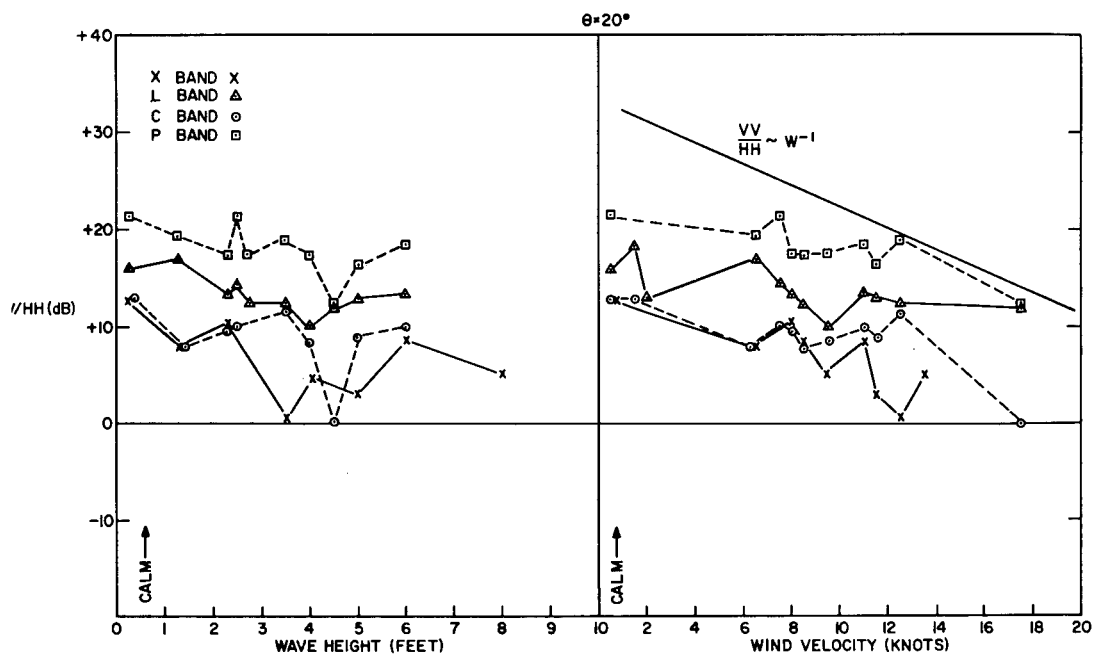


Fig. 16 - Polarization ratio vs surface parameters

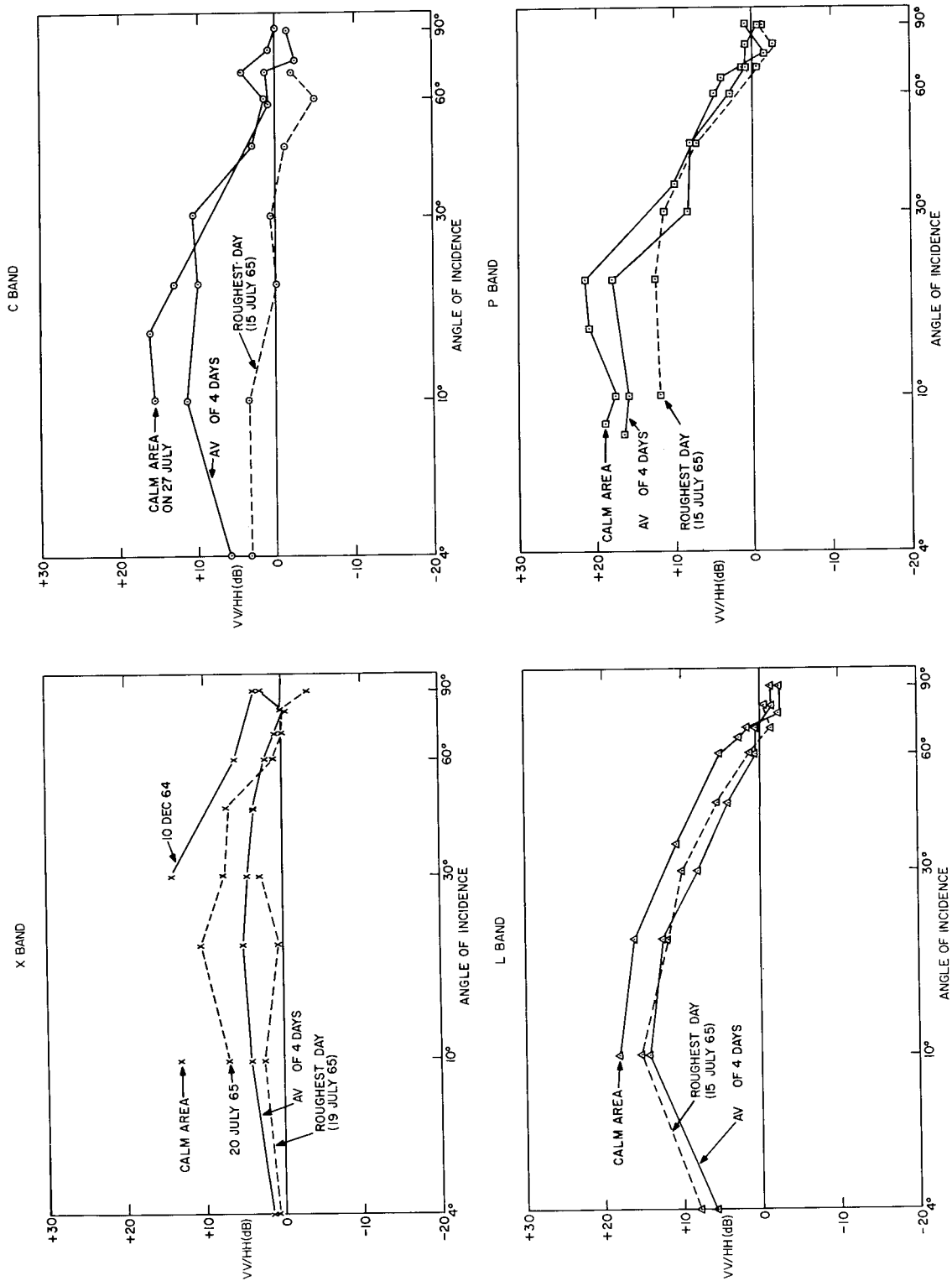


Fig. 17 - Polarization ratio vs wavelength

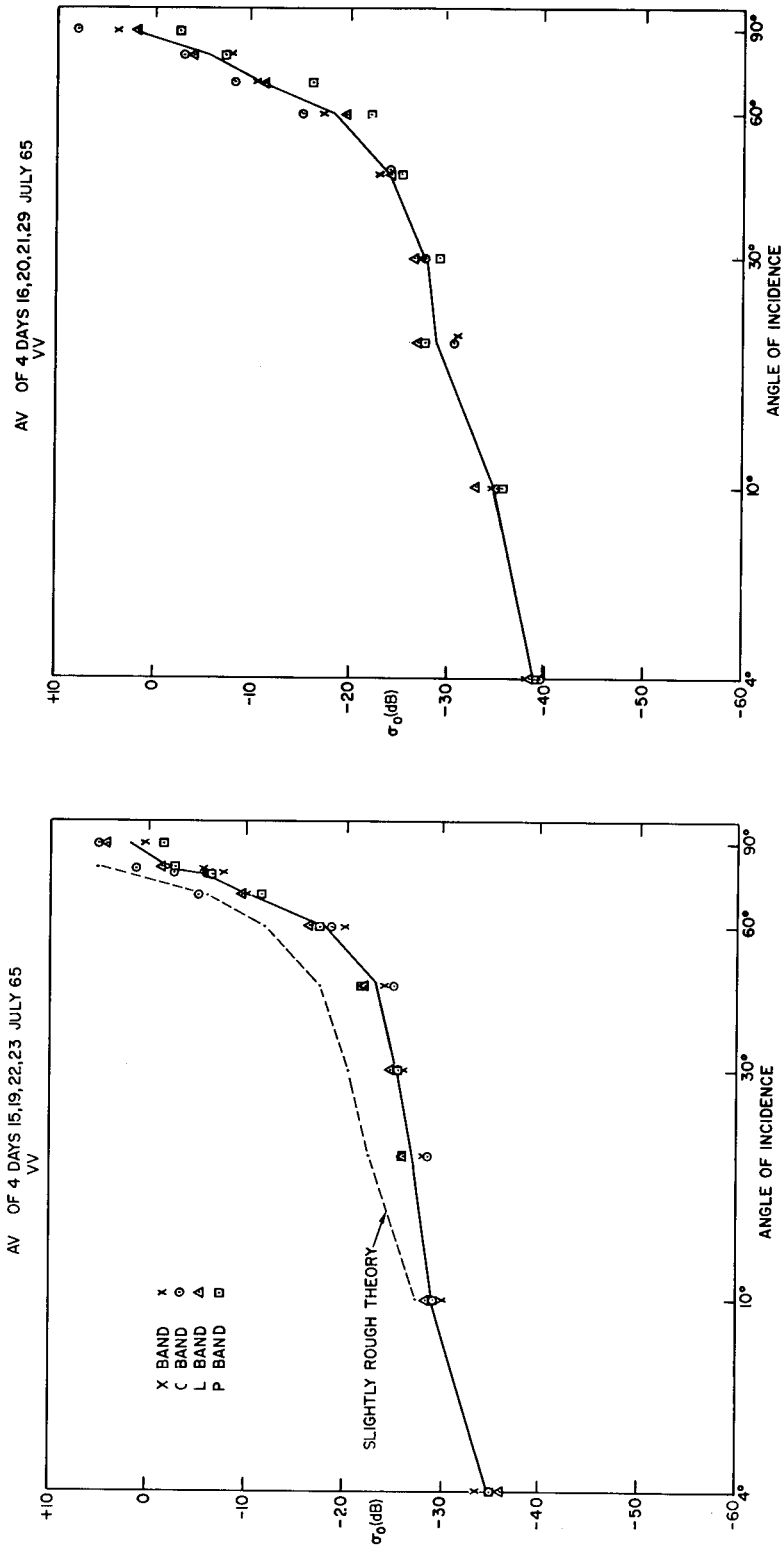


Fig. 18 - Averaged data for VV polarization

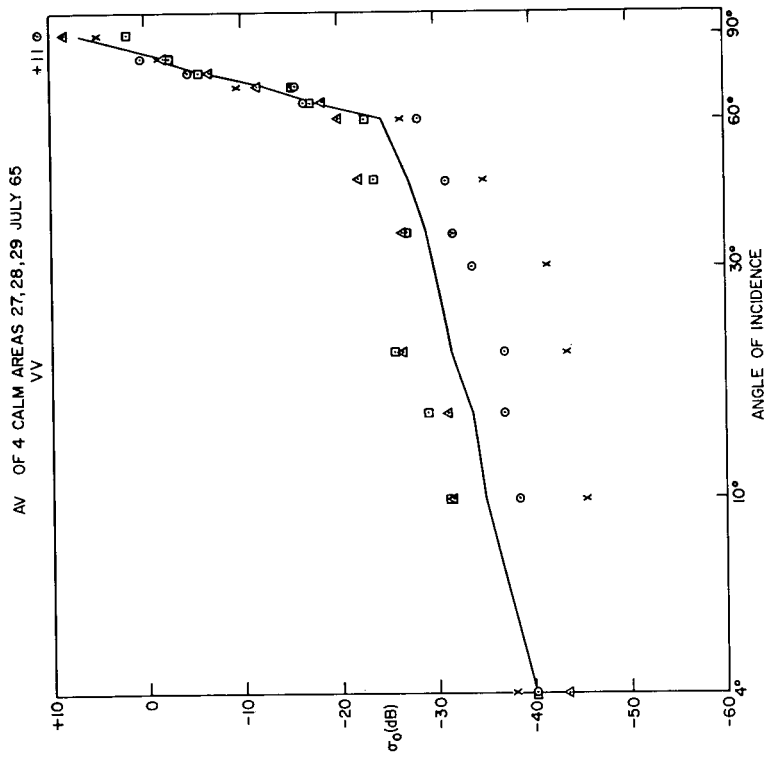


Fig. 18 (continued) - Averaged data for VV polarization

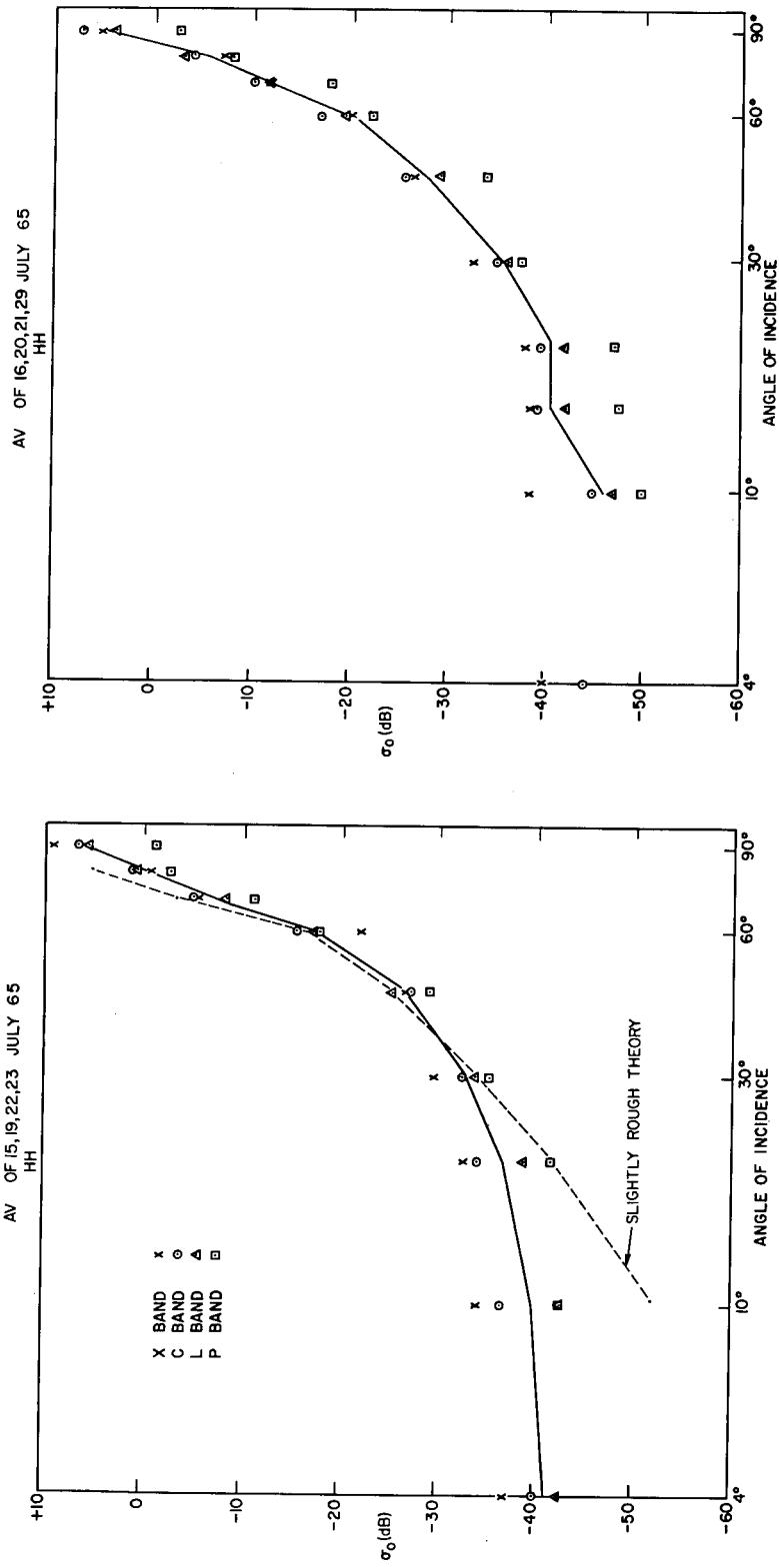


Fig. 19 - Averaged data for HH polarization

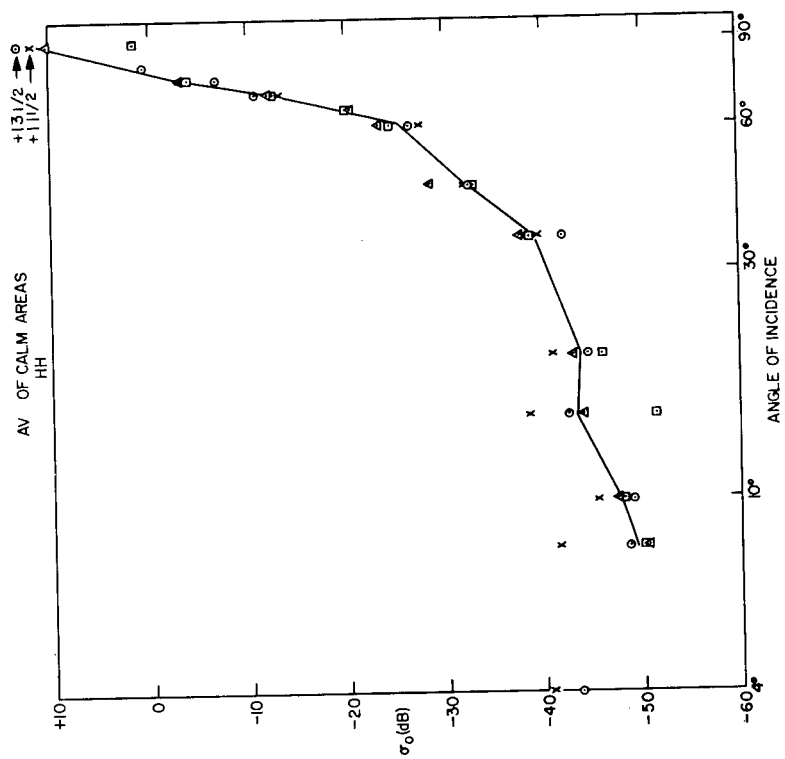


Fig. 19 (continued) - Averaged data for HH polarization

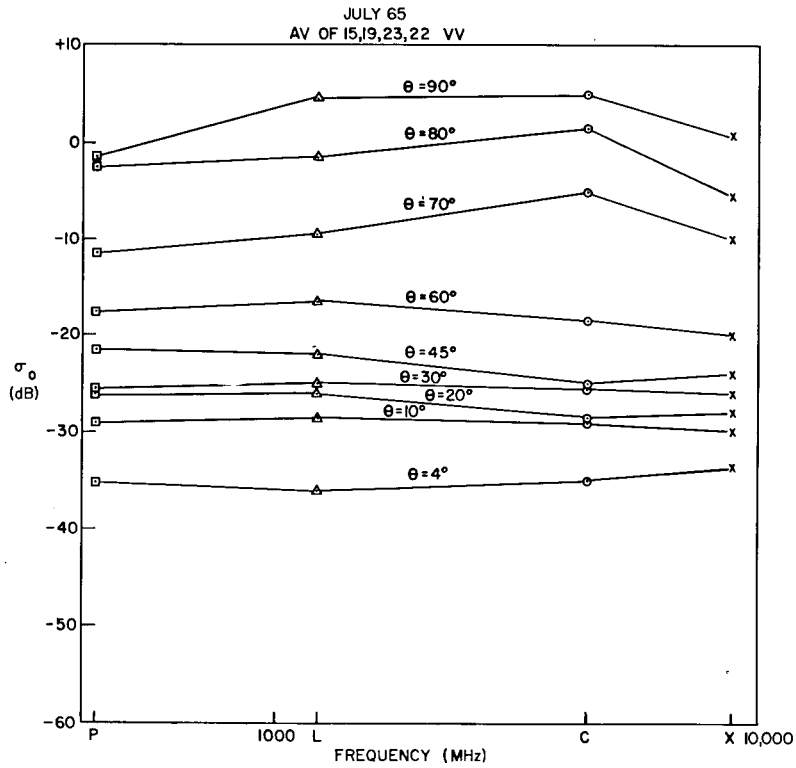
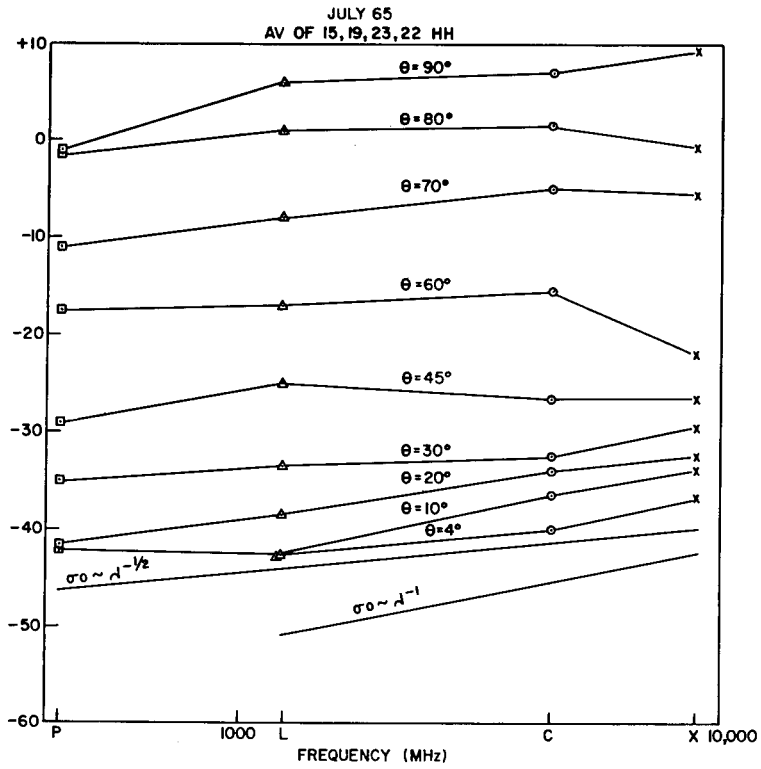


Fig. 20 -  $\sigma_0$  vs wavelength for various values of  $\theta$

Table 4  
Estimates of the Limits of Sphere Measurement Error

Date	Sphere Measurement Error							
	X <sub>V</sub>	X <sub>H</sub>	C <sub>V</sub>	C <sub>H</sub>	L <sub>V</sub>	L <sub>H</sub>	P <sub>V</sub>	P <sub>H</sub>
July 15	±1	None	±1	±1	±1	±1	±1	±1
July 16	±1	None	±1	±1	±1	±1.5	±1	±1
July 19	±1	±1	±1	±1	±1	±1	±1	±1
July 20	±1	±1	±1	±1	±1.5	±1	±1	±1.5
July 21	±1.5	±1.5	±1	±1	±1	±1	±1	±1
July 22	±2	±1	±1	±1	±1.5	±2	±1	±1
July 23	±1	±1.5	±1	±1	±1	±1	±1	±1
July 27	±1	±1	±1	±1	±1	±1.5	±1	±1
July 28	None	±1	±1	None	±1.5	±1.5	None	None
July 29	±2	±2	±2.5	±1	±1.5	±1.5	±1.5	±1.5
Dec 9	±1	±1	±1	None				
Dec 10	±1	±1	±1	None				

## CONCLUSIONS

The initial processing and analysis of radar backscatter data, recorded off the coast of Puerto Rico in July 1965, have been completed at NRL. Radar returns were collected nearly simultaneously on four frequencies on both linear and cross polarizations. The data were processed to obtain the normalized radar cross section  $\sigma_0$  of the sea surface as a function of various parameters. The study of the behavior of the median value of  $\sigma_0$  as a function of the radar parameters and the sea conditions resulted in the following conclusions:

1. The critical angle appears to be independent of sea conditions and radar wavelength for vertical polarization but is a function of both for horizontal polarization.
2. The value of  $\sigma_0$  increases with wind velocity and wave height, with the horizontal polarization case being more sensitive to wind velocity.
3. The polarization ratio decreases with increasing surface roughness and is a function of wavelength.
4. As surface roughness increases, the value of  $\sigma_0$  becomes independent of wavelength for vertical polarization but maintains an inverse wavelength dependence ( $\lambda^{-1}$  →  $\lambda^{-2}$ ) for horizontal polarization.

**FUTURE WORK**

Although the sea conditions covered by the above data are present roughly 60% of the time over all regions of the world, there is reason to measure the behavior of sea clutter for rougher surface conditions. Present theory indicates that wind relations will vanish, the polarization ratio will approach unity on all frequencies, and the value of  $\sigma_0$  in the plateau region will approach a saturation point. It is most desirable to insure that the worst-case clutter conditions have been determined. The collection of clutter data at the highest possible sea states will be attempted in January and February 1969 in the North Atlantic Ocean by the NRL Wave Propagation Branch.

## REFERENCES

1. Kerr, D. E., ed., "Propagation of Short Radio Waves," MIT Rad. Lab. Series, New York:McGraw-Hill, Vol. 13, p. 481, 1951
2. Long, M. W., Wetherington, R. D., Edwards, J. L., and Abelung, A. B., "Wavelength Dependence of Sea Echo," Final Report Project A-840, Eng. Exp. Station, Georgia Tech., July 15, 1965
3. Wilkerson, M. T., and Worsley, P. K. "Introductory Notes on the Measurement and Analysis of Radar Signatures," TRW Systems, June 10, 1963 - Contract #9990-6441-K4-000
4. Dobson, E. B., "Reduction of Data Collected During July 1965 Wave Gauge Experiment in Puerto Rico," APL Memo BPD66U-3, Mar. 9, 1966
5. Dobson, E. B., "Reduction and Analysis of Data from the Ocean Surface Obtained by Stereo-Photography," APL Memo BPD67U-19, Aug. 7, 1967
6. Stilwell, D., "Energy Spectra of the Sea from Photographs," 4th U. S. Navy Symposium on Military Oceanography, Washington, D. C., Proc. Vol. 1, p. 171, Apr. 3-5, 1967
7. Stilwell, D., "Directional Energy Spectra of the Sea from Photographs," Journal of Geophysical Research (to be published)
8. Guinard, N. W., Ransone, J. T., Jr., Laing, M. B., Hearton, L. E., "NRL Terrain Clutter Study, Phase I," NRL Report 6487, May 10, 1967
9. Daley, J. C., "Airborne Radar Backscatter Study at Four Frequencies," NRL Letter Report 5270-20A:JCD:bjg Ser 8560, Aug. 23, 1966
10. Daley, J. C., "Sea Clutter Measurements at X and C Band," NRL Letter Report 5270-18A:JCD:bjg Ser 7287, Aug. 17, 1966
11. Katzin, M., "On the Mechanisms of Radar Sea Clutter," Proc. IRE 45:44-54 (1957)
12. Rice, S.O., "Reflection of Electromagnetic Waves from Slightly Rough Surfaces," Comm. Pure and Appl. Math. 4:351 (1951)
13. Peake, W. H., "Theory of Radar Return from Terrain," IRE Nat. Conv. Record (Part I) 7:27 (1959)
14. Wright, J. W., "A New Model for Sea Clutter," IEEE Trans. for Ant. and Prop. AP-16 (No. 2):217-223 (1968)
15. Valenzuela, G. R., "Depolarization of EM Waves by Slightly Rough Surfaces" IEEE Trans. in Ant. and Prop. Vol. AP-15, No. 4 P552-557, July 1967
16. Durlach, N. I., "Influence of the Earth's Surface on Radar," MIT Lincoln Lab. Tech. Report 373, Jan. 18, 1965

17. Parks, J. K., "Toward a Simple Mathematical Model for Microwave Backscatter from the Sea Surface at Near-Vertical Incidence," IEEE Trans. on Ant. and Prop. AP-12:590-605 (1964)
18. Macdonald, F. C., "Radar Sea Return and Ocean Wave Spectra," Proc. of Conf. on Ocean Wave Spectra, Englewood Cliffs:Prentice-Hall, p. 323-329, 1963
19. Macdonald, F. C., "Sea Clutter at X and L Bands," Unclassified Report in Classified Symposium Record, Univ. of Mich., Feb. 7-9, 1956